HHS Public Access

Author manuscript

Immunity. Author manuscript; available in PMC 2021 January 14.

Published in final edited form as:

Immunity. 2020 January 14; 52(1): 136–150.e6. doi:10.1016/j.immuni.2019.12.006.

Signaling through the inhibitory Fc receptor FcγRIIB induces CD8 T cell apoptosis to limit T cell immunity

Anna B. Morris[1], **Clara R. Farley**[1], **David F. Pinelli**[1,2], **Layne E. Adams**[1], **Mark S. Cragg**[3], **Jeremy M. Boss**[4], **Christopher D. Scharer**[4], **Miguel Fribourg**[5], **Paolo Cravedi**[5], **Peter S. Heeger**[5], **Mandy L. Ford**[1,*]

[1]Department of Surgery, Emory University, Atlanta, GA, USA

[2]Present address: Northwestern University Feinberg School of Medicine, Comprehensive Transplant Center, Division of Transplant Surgery, Chicago, IL

[3]Antibody and Vaccine Group, Cancer Sciences Unit, Faculty of Medicine, University of Southampton, Southampton, UK

[4]Department of Microbiology and Immunology, Emory University, Atlanta, GA, USA

[5]Translational Transplant Research Center and the Precision Institute of Immunology, Icahn School of Medicine at Mount Sinai, New York NY, USA

Summary

Effector $CD8^+$ T cells are important mediators of adaptive immunity, and receptor-ligand interactions that regulate their survival may have therapeutic potential. Here, we identified a subset of effector $CD8^+$ T cells that expressed the inhibitory Fc receptor FcγRIIB following activation and multiple rounds of division. $CD8^+$ T cell-intrinsic genetic deletion of *Fcgr2b* increased $CD8^+$ effector T cell accumulation, resulting in accelerated graft rejection and decreased tumor volume in mouse models. IgG antibody was not required for FcγRIIB-mediated control of $CD8^+$ T cell immunity, and instead, the immunosuppressive cytokine Fgl2 was a functional ligand for FcγRIIB on $CD8^+$ T cells, in that Fgl2 induced caspase 3/7-mediated apoptosis in *Fcgr2b*$^+$ but not *Fcgr2b*$^{-/-}$ $CD8^+$ T cells. Moreover, Increased expression of FcγRIIB correlated with freedom from rejection following withdrawal from immunosuppression in a clinical trial of kidney transplant recipients. Together, these findings demonstrate a cell-intrinsic coinhibitory function of FcγRIIB in regulating $CD8^+$ T cell immunity.

Introduction

Targeting costimulatory and coinhibitory molecules has become an effective therapeutic approach for the treatment of T cell-mediated diseases, including cancer, transplantation, and autoimmunity. Costimulatory receptors are necessary secondary signals for T cell

*Corresponding author and lead contact: Dr. Mandy L. Ford, Professor, Department of Surgery, Emory University, mandy.ford@emory.edu.

Author Contributions

M.L.F. and A.B.M. conceived of the study and wrote the manuscript. P.S.H. conceived of and executed the clinical trial. A.B.M, D.F.P, L.E.A., C.R.F., C.D.S., P.C. performed the research. J.M.B. and M.S.C. provided resources. A.B.M., C.D.S., P.C., and M. L. F. analyzed the data. All authors reviewed and edited the manuscript.

activation, and the constellation of cosignaling molecules expressed on the cell surface serves to calibrate the cell's threshold for activation. Cosignaling receptors also play crucial roles in T cell differentiation and function and impact the outcome of both primary and recall responses. In primary responses, $CD8^+$ T cells expand and differentiate into short-lived effector cells (SLECs) or memory precursor effector cells (MPECs) (Kaech and Cui, 2012). Highly differentiated $CD8^+$ T cells may obviate the requirement for traditional costimulatory pathways, circumventing the typical checkpoints that control $CD8^+$ T cell responses. Because highly differentiated effector T cells are present in many disease processes, including autoimmunity, transplantation, and cancer, understanding the pathways that regulate their function remains an important unanswered question.

Fcγ receptors play a pivotal role in immunity, controlling innate and humoral immunity by actuating the effector functions of antibodies. FcγRIIB is a low-affinity Fcγ receptor well-known to be expressed on B cells, macrophages, DCs, and granulocytes, and is the sole inhibitory Fcγ receptor (Nimmerjahn and Ravetch, 2008). The cytoplasmic domain of FcγRIIB contains an immunoreceptor tyrosine-based inhibitory motif (ITIM) that recruits the inhibitory phosphatase SHIP (Ono et al., 1996), which functions to inhibit phosphorylation of signaling molecules important in activation, including Btk and PLCγ, that disrupt calcium flux through hydrolysis of PIP_3 (Bolland et al., 1998). On innate immune cells, this function of FcγRIIB directly antagonizes activating Fcγ receptors; thus, the balance of activating and inhibitory signals dictates the outcome of the cellular response, similar to cosignaling molecules. On B cells, FcγRIIB is the sole Fcγ receptor (Ravetch et al., 1986); thus, instead of modulating the signaling of activating Fcγ receptors, FcγRIIB-mediated SHIP recruitment functions primarily to attenuate BCR signaling (Ono et al., 1996). In the absence of BCR signaling, however, FcγRIIB signaling promotes apoptosis in a SHIP-independent manner (Pearse et al., 1999). Although early literature suggested T cells might express Fc receptors (Yoshida and Andersson, 1972), (Anderson and Grey, 1974), (Stout and Herzenberg, 1975), the consensus in the field for the past few decades has been that T cells do not express FcγRIIB (Smith and Clatworthy, 2010). Because Fc-containing reagents are increasingly being used therapeutically in transplantation, autoimmunity, and cancer immunotherapy, understanding the role of FcγRs on all cell types is critical to optimize the efficacy of Fc-containing immunotherapeutics in these settings.

Here, we identified a distinct subset of $CD44^{hi}$ $CD8^+$ T cells that expressed FcγRIIB in both mice and humans and in models of both transplantation and tumor immunity. We demonstrated in co-adoptive transfer studies that antigen-specific $CD8^+$ T cells deficient in FcγRIIB exhibited impaired contraction and reduced induction of apoptosis compared to wild-type $CD8^+$ T cells. The impaired attrition observed in FcγRIIB$^{-/-}$ $CD8^+$ T cells was independent of IgG; instead, the immunosuppressive cytokine fibrinogen-like 2 (Fgl2) functioned to induce FcγRIIB-mediated apoptosis in $CD8^+$ T cells. These data thus illuminate a cell-intrinsic role for FcγRIIB as an important modulator of $CD8^+$ T cell responses in vivo.

Results

FcγRIIB is expressed on a subset of effector-memory CD8$^+$ T cells

We assessed the efficacy of the Fc-containing cytotoxic T-lymphocyte antigen-4-Ig (CTLA-4Ig) immunotherapeutic reagent in mice that are genetically deficient in FcγRIIB (Fig. 1A). *Fcgr2b*$^{-/-}$ animals exhibited accelerated rejection of skin allografts as compared to WT animals treated with CTLA-4Ig (Fig. 1B). Because of the known critical role of FcγRIIB in inhibiting B cell activation and antibody production, we hypothesized that this accelerated rejection was due to an unencumbered humoral anti-graft response. However, analysis of donor-specific antibody revealed that in the context of CTLA-4Ig, there was no increase in donor-specific antibody in the *Fcgr2b*$^{-/-}$ recipients as compared to WT hosts (Fig. 1C). Thus, we hypothesized that the rejection-accelerating effect of *Fcgr2b* deficiency must be functioning on some other cell type. Analysis of the T cell response in these animals revealed an increase in the frequency and number of donor-reactive CD8$^+$ T cells (Fig. 1D–E). While it is known that *Fcgr2b* deficiency can enhance antigen-presenting cell (APC) function leading to augmented CD8$^+$ T cell activation (Li et al., 2014), flow cytometric analysis revealed expression of FcγRIIB on CD8$^+$ T cells themselves. In detail, a stringent gating strategy was used to gate on CD4$^+$ and CD8$^+$ CD19$^-$ CD11c$^-$ CD3$^+$ T cells (Fig. 1F), and a distinct population of FcγRIIB-expressing CD8$^+$ cells in aged (>6 months), naïve mice was identified (Fig. 1G–H). Because the anti-CD16/CD32 clone 2.4G2 used for staining binds to both FcγRIIB and FcγRIII, we utilized *Fcgr2b*$^{-/-}$ animals to determine the specificity of staining on CD8$^+$ T cells. In *Fcgr2b*$^{-/-}$ animals, 2.4G2 failed to stain CD8$^+$ T cells, indicating that 2.4G2 binding was specific to FcγRIIB (Fig.1G). This specificity was further confirmed by staining with an FcγRIIB-specific clone (AT130, Fig. S1A). We further queried the expression of FcγRIIB on CD44^{lo}CD62L$^+$ (naïve) cells, CD44^{hi}CD62L$^+$ (Tcm) cells, and CD44^{hi}CD62L^{lo} (Tem) cells and found that the Tem cell subset contained the highest frequencies of FcγRIIB$^+$ cells and that the naïve subset contained the lowest frequencies of FcγRIIB$^+$ cells (Fig. 1I–J). Moreover, the frequency of FcγRIIB-expressing CD44^{hi} CD8$^+$ T cells was highest in the liver, spleen, and bone marrow (Figure 1K–L). These data show that, in contrast to prevailing dogma, FcγRIIB is expressed on a subset of effector/effector memory CD8$^+$ T cells present in both secondary lymphoid organs and in tissues throughout the organism.

FcγRIIB functions intrinsically on CD8$^+$ T cells to limit T cell responses

Given the finding that FcγRIIB was expressed on effector-like CD8$^+$ T cells, we sought to determine whether T cell-expressed FcγRIIB has a functional role on these cells. CD45.2$^+$ *Fcgr2b*$^{-/-}$ OVA-specific (OT-I) T cells were co-transferred at a 1:1 ratio with Thy1.1$^+$ WT OT-I into congenically marked hosts (CD45.1$^+$) (Fig. 2A–B). We then probed the expression of FcγRIIB on WT CD8$^+$ Thy1.1$^+$ OT-I following OVA-expressing skin transplantation and found that the frequency of FcγRIIB$^+$ CD8$^+$ T cells increased over time to constitute ~33% of OT-I T cells at day 21 post-transplant (Fig. 2C). Although WT and *Fcgr2b*$^{-/-}$ OT-I T cells were present at similar frequencies in the spleen on days 4, 7 and 10 post-transplant, by days 14 and 21, *Fcgr2b*$^{-/-}$ OT-I T cells were present at significantly higher frequencies relative to WT OT-I T cells (Fig. 2D–E). The absolute number of *Fcgr2b*$^{-/-}$ OT-I cells was also significantly higher as compared to the number of WT OT-I T cells on days 14 and 21 post-

transplant (Fig. 2F). Given the enrichment of FcγRIIB on $CD44^{hi}CD62L^{lo}$ T cells (Fig. 1J), we compared CD62L expression in the WT vs. *Fcgr2b*$^{-/-}$ OT-I populations. We identified a significant increase in the frequency and number of $CD44^{hi}CD62L^{lo}$ cells on days 14 and 21 in the *Fcgr2b*$^{-/-}$ relative to the WT OT-I T cells (Fig. 2G–I). Similarly, during the contraction phase of the response on days 14 and 21, the frequency and number of *Fcgr2b*$^{-/-}$ $CD44^{hi}CD62L^{+}$ memory $CD8^{+}$ T cells was lower than WT $CD44^{hi}CD62L^{+}$ memory $CD8^{+}$ T cells (Fig. S2A–C). Moreover, *Fcgr2b*$^{-/-}$ OT-I T cells exhibited a significantly higher frequency and number of $Eomes^{lo}Tbet^{hi}$ cells relative to WT OT-I (Fig. 2J–K). This difference was driven mainly by a decrease in Eomes expression in *Fcgr2b*$^{-/-}$ cells, as Tbet expression was not different between WT and *Fcgr2b*$^{-/-}$ OT-I T cells (Fig. 2L and data not shown). These data demonstrate that FcγRIIB has a functional, intrinsic, inhibitory role in limiting the accumulation of differentiated $CD62L^{lo}$ $Eomes^{lo}$ $CD8^{+}$ effector T cells. Given these differences in the accumulation of donor-reactive $CD8^{+}$ T cells, we sought to determine whether $CD8^{+}$ T cell-specific *Fcgr2b* deficiency had a physiologic impact on allograft rejection. WT or *Fcgr2b*$^{-/-}$ OT-I T cells were adoptively transferred into naïve B6 recipients of OVA-expressing skin grafts, which were then treated with costimulation blockade immunosuppression. Importantly, mice containing *Fcgr2b*$^{-/-}$ donor-reactive $CD8^{+}$ T cells exhibited accelerated graft rejection compared to animals containing WT donor-reactive $CD8^{+}$ T cells (Fig. 2M). These data demonstrate that T cell-specific *Fcgr2b* deficiency has a functional, physiologic impact on allograft rejection.

We then sought to assess the T cell intrinsic role of FcγRIIB in response to a tumor model in which naïve B6 recipients of WT or *Fcgr2b*$^{-/-}$ OT-I T cells were inoculated with an OVA-expressing B16 melanoma (Fig. 2N). Assessment of FcγRIIB expression on WT OT-I in this model system revealed that while ~12% of $CD44^{hi}$ tumor antigen (Ag)-specific $CD8^{+}$ T cells isolated from the spleen expressed FcγRIIB, ~27% of $CD44^{hi}$ tumor Ag-specific $CD8^{+}$ T cells isolated from the tumor expressed FcγRIIB by day 14 post tumor inoculation (Fig. S2D–E). The finding that tumor-infiltrating $CD8^{+}$ T cells contained a high frequency of $FcγRIIB^{+}$ cells is corroborated by analysis of graft-infiltrating cells isolated on day 14 following transplantation, which revealed that ~30% of graft-specific $CD8^{+}$ T cells expressed FcγRIIB (Fig. S2H). As in the transplant model, tumor Ag-reactive $FcγRIIB^{+}$ $CD8^{+}$ T cells were more enriched in the Tem cell compartment as compared to naïve or Tcm cells, both in the spleen and tumor (Fig. S2F). Moreover, both the frequency and absolute number of *Fcgr2b*$^{-/-}$ OT-I T cells were significantly elevated relative to WT OT-I T cells at days 10 and 14 following B16-OVA inoculation (Fig. 2O–P). As observed in the transplant model, both the frequency and number of $CD44^{hi}CD62L^{lo}$ cells were significantly increased in the *Fcgr2b*$^{-/-}$ $CD8^{+}$ population relative to the WT $CD8^{+}$ population on day 14 post-tumor inoculation (Fig. 2Q). Importantly, recipients of *Fcgr2b*$^{-/-}$ OT-I T cells exhibited a reduction in tumor volume on days 10 (Fig. S2G) and 14 (Fig. 2R) as compared to recipients of WT OT- I T cells. Taken together, these data illuminate a functional, cell-intrinsic coinhibitory role for FcγRIIB in controlling $CD8^{+}$ T cell responses in models of both transplantation and tumor immunity

FcγRIIB-expressing antigen-specific CD8$^+$ T cells are highly divided and potent cytokine producers

Given the finding that FcγRIIB functions intrinsically on CD8$^+$ T cells, we next sought to identify key differences in expression of cell surface proteins in FcγRIIB$^+$ and FcγRIIB$^-$ OT-I T cell populations at day 14 following skin transplantation using viSNE (Fig. 3A). FcγRIIB-expressing OT-I T cells exhibited a higher mean fluorescent intensity (MFI) of the activation marker CD44, the coinhibitory molecule 2B4, and the costimulatory molecule CD40 and exhibited a lower MFI of CD69 relative to FcγRIIB$^-$ OT-I T cells (Fig. 3B). Furthermore, Cell Trace Violet (CTV)-labeling experiments revealed that antigen-specific CD8$^+$ T cells that had undergone 5 or 6 divisions contained a significantly higher frequency of FcγRIIB-expressing cells compared to CD8$^+$ T cell populations in earlier rounds of division (Fig. 3C–D). Of note, the FcγRIIB$^+$ antigen-specific CD8$^+$ T cell population in the spleen contained a significantly higher frequency of IL-2-, TNF-, and IFN-γ-secreting cells relative to their FcγRIIB$^-$ counterparts (Fig. 3E). Taken together, these data suggest that FcγRIIB$^+$ CD8$^+$ cells are not functionally exhausted but instead are activated, highly divided, and potent cytokine-producing effector cells.

FcγRIIB$^+$ antigen-specific CD8$^+$ T cells exhibit a distinct gene expression profile

To further interrogate the transcriptional program underlying these differences in proliferation and cytokine effector function, RNA-seq was performed on FACS-sorted FcγRIIB$^+$ and FcγRIIB$^-$ antigen-specific CD8$^+$ T cells on day 14 post- transplantation (Fig. 3F). Of note, use of a MACS CD8$^+$ T cell negative selection kit resulted in the preferential depletion of FcγRIIB$^+$ CD8$^+$CD44^{hi}Thy1.1$^+$ OT-I T cells (Fig. S3). 1009 genes were differentially expressed between FcγRIIB$^+$ vs. FcγRIIB$^-$ antigen-specific CD8$^+$ T cells, including *Fcgr2b* (Fig. 3G–H). A number of transcription factors were also differentially expressed between FcγRIIB$^+$ and FcγRIIB$^-$ OT-I T cells (Fig. 3I), as well as many cosignaling molecules (Figure 3J). The gene expression of *Sell* (CD62L) was significantly lower in the FcγRIIB$^+$ OT-I T cells, confirming flow cytometric data which demonstrated that FcγRIIB$^+$ T cells are predominately CD44^{hi}CD62L^{lo} (Fig. 1J) and further that FcγRIIB preferentially regulates CD44^{hi}CD62L^{lo} CD8$^+$ T cells (Fig. 2G–I). Moreover, gene set enrichment analysis (GSEA) revealed that FcγRIIB$^+$ CD8$^+$ T cells are positively enriched in HALLMARK gene sets for allograft rejection, the IL-2-STAT5 signaling pathway, and apoptosis (Fig. 3K). These data show that FcγRIIB$^+$ CD8$^+$ T cells exhibit a distinct gene expression profile as compared to FcγRIIB$^-$ CD8$^+$ T cells, one that is indicative of highly potent, multi-functional effector T cells.

FcγRIIB inhibits CD8$^+$ T cell responses by inducing active caspase 3/7 in a cell intrinsic manner

Given the GSEA signature suggesting altered apoptosis, along with the observation that *Fcgr2b*$^{-/-}$ CD8$^+$ T cells exhibited enhanced survival during the contraction phase of the response, we hypothesized that FcγRIIB was functioning to inhibit Ag-specific CD8$^+$ T cell accumulation by inducing apoptosis. To test this, we first measured active caspase 3/7 expression in FcγRIIB$^+$ vs. FcγRIIB$^-$ Ag-specific CD8$^+$ T cells at day 16 post-transplant. Results indicated a marked increase in the frequency of active caspase 3/7$^+$ cells within the

FcγRIIB$^+$ subset relative to the FcγRIIB$^-$ subset (Fig. 3L–M). To determine whether this impact of FcγRIIB deficiency on Ag-specific CD8$^+$ T cell apoptosis was T cell intrinsic, we co-adoptively transferred WT and *Fcgr2b*$^{-/-}$ OT-I T cells into congenic hosts and measured the frequency of caspase 3/7$^+$ apoptotic cells at day 16 post-transplant. Results indicated a significant reduction in the frequency of active caspase 3/7$^+$ T cells within the *Fcgr2b*$^{-/-}$ vs. WT CD8$^+$ Ag-specific transferred cells (Fig. 3N–O), suggesting that FcγRIIB-mediated signals result in CD8$^+$ T cell apoptosis.

Immunotherapy with anti-FcγRIIB functions to augment CD8$^+$ T cell responses in vivo

Because these data indicated that FcγRIIB functions as a cell-intrinsic coinhibitor of CD8$^+$ T cells, we sought to determine whether FcγRIIB could be pharmacologically targeted to manipulate alloreactive CD8$^+$ T cell responses in vivo. Naïve B6 animals received adoptive transfers of Thy1.1$^+$ OT-I T cells and Thy1.1$^+$ CD4$^+$ OVA-specific (OT-II) T cells along with OVA-expressing skin grafts and were then treated with an FcγRIIB-specific antagonistic monoclonal antibody (AT-128) (Fig. 4A). This FcγRIIB-blocking antibody has shown to be non-cross-reactive with other FcRs (Williams et al., 2012). Analysis of the T cell response in the spleens of anti-FcγRIIB-treated recipients on day 14 post-transplant revealed a significant increase in both frequency and number of antigen-specific Thy1.1$^+$ CD8$^+$ T cells as compared to untreated controls (Fig. 4B–C), demonstrating that pharmacologic antagonism of FcγRIIB functions to augment antigen-specific CD8$^+$ T cell responses in vivo. Moreover, blockade of the FcγRIIB pathway impacted CD8$^+$ T cell apoptosis, in that the frequency of active caspase 3/7$^+$ 7-AAD$^+$ antigen-specific Thy1.1$^+$ CD8$^+$ T cells was significantly lower in animals treated with anti-FcγRIIB relative to untreated controls (Fig. 4D–E). These data demonstrate that FcγRIIB can be pharmacologically manipulated, and suggest it requires ligand binding in order to control CD8$^+$ T cell responses in vivo.

It is worth noting that we also addressed the impact of blockade of the FcγRIIB pathway on antigen-specific CD4$^+$ T cell responses in this system. Results indicated that antibody blockade of FcγRIIB resulted in a significant increase in both the frequency and number of graft-specific CD4$^+$ OT-II T cells (Fig. S4A–C). However, as demonstrated in Fig. 1G–J, we failed to detect FcγRIIB expression on CD4$^+$ T cell populations. The ability of FcγRIIB deficiency to secondarily increase T cell responses via its effect on DC has previously been demonstrated by Ravetch's group (Li et al., 2014). Thus, in order to determine if there is any contribution of CD8$^+$ T cell-expressed FcγRIIB on the contemporaneous CD4$^+$ T cell response, we assessed the tumor-reactive CD4$^+$ OT-II T cell response in animals that had received either WT or *Fcgr2b*$^{-/-}$ CD8$^+$ OT-I T cells (Fig S4D–F). Results indicated that there was no difference in either the frequency or number of tumor-specific OT-II T cells in recipients of WT vs. *Fcgr2b*$^{-/-}$ CD8$^+$ T cells. Taken together, these results suggest that the impact of FcγRIIB blockade to augment CD4$^+$ T cell responses is likely functioning primarily through its effect on APC. They further demonstrate that the accelerated rejection observed in skin graft recipients containing *Fcgr2b*$^{-/-}$ vs. WT CD8$^+$ OT-I T cells (Fig. 2M) is not due to secondary effects on the graft-specific CD4$^+$ T cell population.

IgG antibodies are not required for FcγRIIB-mediated control of CD8+ T cell responses

The results presented above demonstrate that ligand binding is required for the ability of FcγRIIB to regulate the survival of potent, differentiated $CD8^+$ effectors. However, the nature of the ligand was unknown. Thus, we next addressed the requirement for IgG antibody in FcγRIIB-mediated control of $CD8^+$ T cell responses. WT graft-specific OT-I T cells were adoptively transferred into either WT or *Aicda*$^{-/-}$ animals, which lack the ability to class-switch and thus have a complete absence of endogenous IgG (Fig. 5A) (Muramatsu et al., 2000; Robbiani et al., 2008). WT or *Aicda*$^{-/-}$ recipients were transplanted with OVA-expressing skin grafts and then were left untreated or were treated with anti-FcγRIIB (2.4G2). Results indicated that the ability of anti-FcγRIIB to enhance donor-reactive $CD8^+$ T cell responses was preserved in *Aicda*$^{-/-}$ hosts (Fig. 5B). To confirm these results in the setting of $CD8^+$ T cell-specific FcγRIIB deficiency, WT vs. *Fcgr2b*$^{-/-}$ OT-I T cells were adoptively transferred into WT or *Aicda*$^{-/-}$ hosts, which received OVA-expressing skin grafts and were sacrificed on day 21 post-transplant. Importantly, results indicated that the augmented accumulation of *Fcgr2b*$^{-/-}$ vs. WT $CD8^+$ T cells is still observed when animals lacked IgG (Fig. 5C). These data demonstrate that antibody binding is not required for the observed ability of cell-intrinsic *Fcgr2b* deficiency to increase $CD8^+$ T cell responses, and suggest that antibodies are not the functional ligand by which FcγRIIB controls $CD8^+$ T cells.

Fibrinogen-like 2 (Fgl2) induces CD8+ T cell apoptosis in an FcγRIIB-dependent manner

Given the results that IgG is not required for FcγRIIB-mediated control of $CD8^+$ T cell responses, we queried other potential FcγRIIB ligands. Fibrinogen-like 2 (Fgl2) is an anti-inflammatory cytokine produced by many cell types, most prominently $Foxp3^+$ Treg (Joller et al., 2014), and has been shown to ligate FcγRIIB on dendritic cells and macrophages (Liu et al., 2008). However, a direct role for Fgl2 in controlling $CD8^+$ T cell responses via FcγRIIB has not been investigated. To begin to assess the ability of Fgl2 to bind to FcγRIIB on $CD8^+$ T cells in the setting of transplantation, soluble Fgl2 (sFgl2) protein was first measured in the serum in naïve and grafted animals. Data show an increase in serum concentration of sFgl2 protein on day 21 post-transplant relative to day 3 post-transplant (Fig. S2I). Surface Fgl2 binding was next assessed on FcγRIIB$^+$ vs. FcγRIIB$^-$ $CD44^{hi}$ $CD8^+$ T cells obtained from grafted mice at day 14 post-transplant. Results revealed that FcγRIIB$^+$ $CD8^+$ T cells contained a markedly greater frequency of cells that also stained positively for Fgl2 surface expression, relative to FcγRIIB$^-$ $CD8^+$ T cells (Fig. 5D). Moreover, Fgl2$^+$ FcγRIIB$^+$ $CD8^+$ cells exhibited a significant increase in active caspase 3/7 relative to Fgl2$^-$ FcγRIIB$^+$ $CD8^+$ T cells, suggesting that ligation of FcγRIIB by Fgl2 was associated with an increase in apoptosis in $CD8^+$ T cells (Fig. 5E).

To determine whether Fgl2 physically ligates FcγRIIB on $CD8^+$ T cells, we tested whether pre-incubation with 2.4G2 blocked binding of Fgl2. Results indicated that pre-incubation with 2.4G2 significantly diminished staining of Fgl2 relative to cells that were pre-incubated with media alone (Fig. 5F–G). Moreover, Fgl2 was unable to bind *Fcgr2b*$^{-/-}$ $CD8^+$ T cells, and there was no effect of pre-incubation with 2.4G2 (Fig. 5F–G). In aggregate, these data show that Fgl2 physically ligates FcγRIIB on $CD8^+$ T cells. Next, to determine whether Fgl2 can serve as a functional ligand for FcγRIIB and induce apoptosis in FcγRIIB-

expressing $CD8^+$ T cells, WT vs. *Fcgr2b*$^{-/-}$ $CD8^+$ T cells were first stimulated with cognate antigen for 2 days ex vivo and then cultured in the presence or absence of recombinant Fgl2 for 24 hours. Data demonstrate that the addition of Fgl2 resulted in a significantly increased frequency of active caspase $3/7^+$ 7-AAD^+ cells among WT $CD8^+$ T cells, but not among *Fcgr2b*$^{-/-}$ $CD8^+$ T cells (Fig. 5H–I). These data demonstrate that Fgl2 is a functional ligand by which FcγRIIB controls $CD8^+$ T cell apoptosis.

FcγRIIB is expressed on human $CD8^+$ T cells and is associated with freedom from rejection following withdrawal of tacrolimus immunosuppression in human renal transplant recipients

In order to assess the potential clinical relevance of these results, we next queried the expression of FcγRIIB on $CD8^+$ T cells isolated from both normal healthy controls and from transplant recipients. PBMC from healthy volunteers and from 4 transplant recipients were isolated in an IRB-approved protocol and are gated on $CD8^+$ T cells. Cells were stained with anti-FcγRII (clone FUN-2). Results indicate that anti-FcγRII stained human $CD8^+$ T cells in both normal healthy controls and in transplant recipients (Fig. 6A–B). While we observed a range of frequencies of positive cells within the $CD8^+$ T cells compartments between individuals, the average frequency among transplant recipients was significantly lower as compared to normal healthy controls (Fig. 6C). To confirm that specifically FcγRIIB is expressed on human $CD8^+$ T cells, we isolated PBMC from 7 healthy volunteers and from 4 pre-transplant recipients and FACS-sorted (97%) for $CD19^-CD14^-CD3^+CD4^-$ $CD8^+$ T cells (Fig. 6A, D). RNA was then extracted for qPCR analysis for *FCGR2B*. Results indicate that human $CD8^+$ T cells in both normal healthy controls and in transplant recipients express ~400- fold greater *FCGR2B* mRNA than $CD4^+$ T cells (Fig. 6E).

Given these data showing that human $CD8^+$ T cells express FcγRIIB, we queried whether increased expression of FcγRIIB might portend better outcomes by limiting the alloreactive $CD8^+$ T cell response post-transplantation. We interrogated the association of FcγRIIB with transplant rejection and the development of new donor specific antibodies in a subset of renal transplant recipients as part of the CTOT-09 clinical trial (Hricik et al., 2015) (Fig. 6F). In brief, 14 clinically stable subjects 6-months post-transplant were randomized to be weaned off of tacrolimus immunosuppression (but remained on low doses of steroids and mycophenolic acid). RNA from PBMC samples was obtained prior to initiating the tacrolimus withdrawal. Eight of the 14 subjects developed donor-specific antibody or acute cellular and/or antibody rejection following weaning of tacrolimus, while the remaining six were stable (without rejection, donor specific antibody or changes in kidney function) for the duration of the 18-month follow up period. Transcript analysis of pre-withdrawal PBMC revealed only eight differentially expressed genes between those that developed evidence of transplant dysfunction and those that were stable. Of these, seven genes were upregulated and one was downregulated in the patients that remained stable following immunosuppression withdrawal (Fig. 6G). *FCGR2B* was one of the genes that was significantly higher in patients who were rejection-free off tacrolimus immunosuppression as compared to those who developed alloantibodies, cellular or humoral graft rejection following withdrawal from tacrolimus (Fig. 6H). CellCODE analysis, which quantifies the

strength of relationships between canonical gene sets of distinct immune cell lineages and a gene of interest, was then used to assess the strength of the association between *FCGR2B* expression and B cells, $CD4^+$ T cells, $CD8^+$ T cells, DCs, monocytes, and NK cells (Chikina et al., 2015). In brief, CellCODE corrects for cell mixture variation in data sets using a latent variable approach to reliably estimate proportions of cells using publicly available homogeneous datasets in the form of surrogate proportion variables (SPVs) and is used to perform cell type deconvolution in transcriptomic data analyses with high accuracy (Chikina et al., 2015). Several recent high-impact studies have employed the CellCODE bioinformatics approach in lieu of traditional cell-sorting to assess cell-type specific gene expression patterns (Altman et al., 2019; Hartmann et al., 2017; Lee et al., 2018; Liu et al., 2019). Using this platform, we found that *FCGR2B* mRNA expression was highest in B cells, dendritic cells, and monocytes, findings which are consistent with our flow cytometry data (not shown), thus validating the successful application of CellCODE. Using an interaction model, we queried which cell lineage was most tightly associated with the differences in *FCGR2B* mRNA expression between the stable and rejecting patients at time of tacrolimus withdrawal. The F-statistic derived from these analyses was the highest for $CD8^+$ T cells, indicating that *FCGR2B* mRNA expression in the $CD8^+$ T cell subset drives the differences observed between stable vs. rejected patients (Fig. 6I). We then compared the original list of 8 genes that were differentially expressed between stable vs. rejecting transplant patients in this trial against our RNASeq data set comparing FACS-sorted $Fc\gamma RIIB^+$ vs. $Fc\gamma RIIB^-$ $CD8^+$ T cells. Of note, of the 7 remaining transcripts that were upregulated in the stable patients, 3 of them were significantly upregulated in FACS-purified $Fc\gamma RIIB^+$ T cells relative to $Fc\gamma RIIB^-$ $CD8^+$ T cells (*Cpa3*, *Gm2a*, *Skap2*) (Fig. 6J). These data further support the conclusion that it is $Fc\gamma RIIB$ on $CD8^+$ T cells that underlies the differential expression observed in rejecting vs. stable transplant recipients.

Discussion

Here we show that $Fc\gamma RIIB$ functions intrinsically to inhibit murine and human $CD8^+$ T cell responses. These studies challenge long-held dogma that T cells do not express Fc receptors (Nimmerjahn and Ravetch, 2008). Instead, our data corroborate recent studies demonstrating $Fc\gamma RIIB$ mRNA in and protein expression on $CD8^+$ T cells (Alfei et al., 2019; Starbeck-Miller et al., 2014; Wirth et al., 2010). Importantly, the mRNA expression of $Fc\gamma RIIB$ excludes the possibility that the observed $Fc\gamma RIIB$ is solely due to the acquisition of $Fc\gamma RIIB$ protein from other cells. The results presented here suggest that under physiologic conditions, $Fc\gamma RIIB$ inhibits the survival of $CD8^+$ T cells. In line with this hypothesis, we show that $Fc\gamma RIIB^+$ antigen-specific $CD8^+$ T cells exhibit gene set enrichment in apoptosis. These data suggest that $Fc\gamma RIIB$ modulates apoptosis signaling pathways in $CD8^+$ T cells, similar to one of the reported functions of $Fc\gamma RIIB$ on B cells (Ono et al., 1996). The ability of $Fc\gamma RIIB$ to induce apoptosis in $CD8^+$ T cells is biologically significant, in that $CD8^+$ T cell-specific *Fcgr2b* deficiency resulted in accelerated allograft rejection and decreased tumor load in mouse models of transplantation and melanoma, respectively, and in that increased $CD8^+$ T cell-associated $Fc\gamma RIIB$ correlated with rejection-free allograft survival in a cohort of renal transplant recipients. These data therefore demonstrate that $Fc\gamma RIIB$ is

an important, overlooked intrinsic regulator of $CD8^+$ T cell responses in both mouse and humans.

Our study also provides insight into the mechanisms by which FcγRIIB regulates $CD8^+$ T cell immunity. We showed that FcγRIIB functionality on $CD8^+$ T cells is controlled by ligation of a binding partner; however, the most well-known FcγRIIB ligand, IgG antibody, is not required for the ability of FcγRIIB to regulate $CD8^+$ T cell responses. Instead, our results implicated Fgl2 as the functional ligand via which FcγRIIB signaling induces apoptosis in $CD8^+$ effector T cells. Together, these data provide conceptual insight into the physiologic role of the FcγRIIB pathway on $CD8^+$ T cells. As shown in Fig. 3C–E, FcγRIIB is upregulated after the 6^{th} division and persists on differentiated effector-memory $CD8^+$ T cells that have potent effector function. It is known that systemic serum Fgl2 protein concentration is increased in settings of chronic inflammation including cancer (Latha et al., 2019; Tang et al., 2017; Yan et al., 2015; Yan et al., 2019; Zhu et al., 2017) and chronic viral infection (Foerster et al., 2010; Marsden et al., 2003), and here we have shown that Fgl2 induces apoptosis of $Fc\gamma RIIB^+$ $CD8^+$ T cells. Thus, these data suggest that the physiologic relevance of this pathway is to allow for control of active, highly differentiated effectors in the setting of chronic inflammation in order to limit immune pathology. FcγRIIB/Fgl2 interactions are thus a potential therapeutic target for controlling $CD8^+$ T cells that has clinical applicability in cancer, infection, transplantation, and autoimmunity.

The data presented here indicate that Fgl2 is a functional ligand for FcγRIIB on $CD8^+$ T cells resulting in apoptosis, and not that Fgl2 binds to some other receptor expressed on a subset of $Fc\gamma RIIB^+$ T cells and induces apoptosis. This conclusion is supported by our findings that 1) pre-incubation with anti-FcγRIIB blocks Fgl2 binding and 2) Fgl2 binding is absent on *Fcgr2b*$^{-/-}$ $CD8^+$ T cells. However, only a subset of $Fc\gamma RIIB^+$ T cells (~10%) stain positive for Fgl2, raising the possibility that FcγRIIB requires a specific modification for Fgl2 binding which occurs only a subset of $Fc\gamma RIIB^+$ cells. Given our results that IgG antibody was not required for the induction of apoptosis in $Fc\gamma RIIB^+$ $CD8^+$ T cells, it is possible that some modification of $Fc\gamma RIIB^+$ may render it unable to bind IgG and instead able to bind Fgl2 to induce apoptosis. In support of this notion, ~80% of $Fc\gamma RIIB^+$ cells that were able to bind Fgl2 stained positive for markers of apoptosis. Of course, these findings do not preclude the existence of other ligands for FcγRIIB on $CD8^+$ T cells. Future studies to explore the range of responses of $Fc\gamma RIIB^+$ $CD8^+$ T cells to both endogenous and pharmacologic ligands are ongoing.

Further bolstering the notion that FcγRIIB modulates $CD8^+$ T cell survival, we observed a tight relationship between FcγRIIB-expressing cells and effector-like phenotypes, including the observations that $Fc\gamma RIIB^+$ cells are highly enriched in the effector memory population, are potent cytokine producers, and have undergone multiple rounds of division. Moreover, $Fc\gamma RIIB^+$ cells have lower transcripts of CD62L and the transcription factor Eomes, suggesting that FcγRIIB ligation may induce a negative signal in $CD44^{hi}CD62L^{lo}$ and $Eomes^{lo}$ short-lived effector T cells that are then programmed for deletion. Mechanistically, this deletion may proceed through the cell-intrinsic apoptotic pathway, as $Fc\gamma RIIB^+$ $CD8^+$ T cells contain a higher frequency of cells that stain positively for active caspase 3/7. Furthermore, we found that pharmacologic targeting of FcγRIIB resulted in an

accumulation of CD44^{hi}CD62L^{lo} cells and that *Fcgr2b*$^{-/-}$ antigen-specific CD8^{+} T cells are enriched in CD44^{hi}CD62L^{lo} and Eomes^{lo} cells. These data confirm that FcγRIIB preferentially inhibits CD44^{hi}CD62L^{lo} and Eomes^{lo} cells. Because Eomes and CD62L are canonical molecules associated with high-quality memory T cell differentiation (reviewed in (Kaech and Cui, 2012)), these data suggest that FcγRIIB functions to inhibit highly potent effector cells.

Why has FcγRIIB expression on T cells not been well-characterized before now? Of note, FcγRIIB is not present on naïve T cells (Fig. 1I–J). FcγRIIB upregulation becomes most prevalent during the contraction phase at day 14 and 21. As cells are contracting quickly, smaller numbers might make it difficult to detect FcγRIIB-expressing cells. Further, the MFI of FcγRIIB is lower on T cells than it is on B cells (data not shown), and to obtain clear, interpretable staining, we utilized a biotinylated antibody to amplify the signal. Moreover, we found that FcγRIIB^{+} OT-I T cells were depleted following the use of a negative selection CD8^{+} MACS enrichment kit (Fig. S3), raising the issue that any study enriching for CD8^{+} in this manner would likely exclude this subset of T cells, potentially biasing the results of the study.

The potential implications of T cells expressing Fcγ receptors are profound. As we move into the era of biologics to treat human disease (which have the potential to interact with Fc receptors, either in harmful or beneficial ways), elucidating the coinhibitory role of FcγRIIB on T cells is critical for complete understanding of how these reagents work and why they sometimes fail. Further, the identification of the role of Fgl2 in inhibiting the accumulation of effector CD8^{+} T cells demonstrate a regulatory interaction between innate and adaptive aspects of immunity. Therapeutic modulation of this inhibitory pathway could be applied to mitigate T cell-mediated diseases, including transplant rejection, tumor immunity, autoimmunity, and protective immunity against pathogens.

STARMethods

LEAD CONTACT AND MATERIALS AVAILABILITY

Further information and requests for resources and reagents should be directed to and will be fulfilled by the Lead Contact, Mandy Ford (mandy.ford@emory.edu).

There are restrictions related to the availability of the *Fcgr2b*$^{-/-}$ OT-I mice generated in this study, the anti-CD28 domain antibodies used, and the AT128 antibodies used due to the limitations of the MTAs through which we obtained these reagents.

EXPERIMENTAL MODEL AND SUBJECT DETAILS

Mice—Male C57BL/6 (H-2b) and B6/Ly5.2 mice aged 6–8 weeks were obtained from the National Cancer Institute (Frederick, MD). OT-I (Hogquist et al., 1994) and OT-II (Barnden et al., 1998) transgenic mice were purchased from Taconic Farms (Germantown, NY) and bred to Thy1.1^{+} background at Emory University. OVA-transgenic mice (C57BL/6 background, H-2b) (Ehst et al., 2003) were a generous gift from Dr. Marc Jenkins (University of Minnesota, Minneapolis, MN). B6;129S-Fcgr2b^{tm1Ttk}/J (*Fcgr2b*$^{-/-}$) were purchased from The Jackson Laboratory (stock #002848, (Takai et al., 1996)). These mice

were used in Fig. 1. EM:06078 Fcgr2b Fcgr2bB6null B6(Cg)-Fcgr2btm12Sjv/Cnbc (or *Fcgr2b*$^{-/-}$) mice were purchased from the European Mutant Mouse Archive (EMMA) and provided by the Academisch Siekenhuis Leiden/Leiden University Medical Center from Dr. J.S. Verbeek (Boross et al., 2011). These mice were generated using embryonic stem cells from B6 mice and used in Fig. 2, 3, 5, S2, and S4. *Fcgr2b*$^{-/-}$ mice from EMMA were bred to OT-I transgenic mice at Emory University for use in intrinsic experiments to exclude any T cell effects of the 129 background. B6.129P2-Aicda$^{tm1(cre)Mnz}$/J (*Aicda*$^{-/-}$) mice were purchased from The Jackson Laboratory (stock #007770). Unless otherwise stated in the figure legend and text, mice were aged 8 weeks at the start of the experiment, experimental hosts were male, and donor animals for adoptive transfers and skin transplantation were male or female. This study was carried out in strict accordance with the recommendations in the Guide for the Care and Use of Laboratory Animals. The protocol (PROTO201700558) was approved by the Institutional Animal Care and Use Committee of Emory University. All surgery was performed under general anesthesia with maximum efforts made to minimize suffering. All animals were housed in specific pathogen-free animal facilities at Emory University.

Human subjects—Patients undergoing renal transplantation at Emory University Hospital between the years 2009 and 2015, as well as normal healthy controls, were enrolled in an immune monitoring protocol approved by Emory University's Institutional Review Board (IRB #00046593) after informed consent was obtained. Patient samples for this study were acquired prior to transplantation (baseline).

Healthy and transplant recipients for flow cytometry: Of the 5 healthy controls, there were 3 males and 2 females, age range 22–63. Of the 4 transplant recipients, there were 3 males and 1 female, age range 22–79.

Healthy and transplant recipients for qPCR: Of the 4 healthy controls, there were 2 males and 2 females, age range 52–62. Of the 4 transplant recipients, there were 2 males and 2 females, age range 26–69.

CTOT09 clinical trial: The CTOT09 study included 21 living donor renal transplant recipients who received anti-thymoglobulin (ATG), mycophenolate mofeteil (MMF), steroids, and tacrolimus and were without rejection, development of donor-specific antibody (DSA), or BK virus (BKV) for 6 months and had normal protocol biopsies at 6–7 months post-transplant. Seven of these patients were randomized to stay on tacrolimus, MMF, and steroids while 14 patients underwent withdrawal from tacrolimus immunosuppression over a 2-month period. There were no differences in age (range= 37–61 for control group, range= 24–73 for tacrolimus withdrawal group, p=0.79) or sex (p=0.66) between the two groups (Hricik et al., 2015). RNA was isolated from PBMC samples taken prior to initiating withdrawal. Of the 14 patients who underwent withdrawal from immunosuppression, eight developed donor-specific antibody or acute cellular rejection, while six did well for the duration of the 18-month follow up period off of tacrolimus immunosuppression.

METHOD DETAILS

Adoptive cell transfers—To monitor antigen-specific donor-reactive $CD8^+$ T cell responses, we used our previously described system in which OVA-specific transgenic T cells in naïve animals are adoptively transferred prior to skin transplantation with OVA-expressing skin. For the adoptive transfer, WT OT-I, *Fcgr2b*$^{-/-}$ OT-I, and OT-II transgenic cells were harvested from the spleen and mesenteric lymph nodes. Cells were counted using a Nexcelom Cellometer Auto T4 (Nexecelom Bioscience, Lawrence, MA) and stained with CD8- BV785, CD4- PacBlue, Thy1.1- PerCP, Vα2- FITC, and Vβ5- PE (BioLegend). Frequency of OT-I and OT-II was determined via Vα2 and Vβ5 TCR co-expression. Cells were resuspended in 1X PBS and adoptively transferred into naïve hosts 24 hours prior to skin transplantation or B16-OVA melanoma inoculation. Where indicated, OT-I T cells were labeled with 5uM CellTrace Violet (CTV) dye (Life Technologies, Invitrogen) according to manufacturer's instructions and then adoptively transferred into naïve hosts. Proliferation was measured on day 14 post transplantation via flow cytometry on a BS LSR II (BD Biosciences) and data were analyzed with FlowJo (Tree Star, San Carlos, CA) and Prism (GraphPad Software).

Antigenic challenges—Mice were transplanted with full thickness (~1cm) tail, ear, or trunk skins from transgenic OVA-expressing mice on the dorsal thorax and wrapped with adhesive bandages for seven days (Trambley et al., 1999). For tumor challenge, mice were inoculated with 10^6 B16-OVA melanoma cells in the subcutaneous tissue of the right flank. The B16 melanoma cell line engineered to express the OVA epitope was provided by Dr. Yang-Xin Fu (Brown et al., 2001). Tumor growth was then followed by daily visual inspection. Tumor volume was calculated using caliper measurement of height, width and depth.

Where indicated, mice were treated intraperitoneally with 250ug CTLA-4Ig (abatacept, Bristol Myers-Squibb) on days 0, 2, 4, and 6, 50ug CD28 domain antibody (anti-CD28dAb, Bristol Myers-Squibb) on days 0, 2, 4, 6, and every other day thereafter until day 30, 250ug CD32B (Clone: AT128) provided by Dr. Mark Cragg (Williams et al., 2012) on days 6, 8 and 10, or with 250ug CD16/CD32 (Clone: 2.4G2, BioXCell, West Lebanon, NJ) on days 6, 8 and 10. Grafts were considered rejected when less than 10% of viable graft remained.

ELISAs—For the anti-OVA IgG ELISA, 96-well plates were incubated overnight with 10ug/mL OVA protein in coating buffer. Wells were blocked with blocking buffer (PBS + 0.2% Tween-20 + 10% FBS) for 30 minutes at room temperature (RT), and serial dilutions of serum were added to each well and incubated for 90 minutes at 37C. Plates were then washed three times in PBS + 0.5% Tween-20. A 1:1000 dilution of biotinylated anti-IgG was then added and incubated for 30 minutes at RT. Plates were then washed three times in PBS + 0.5% Tween-20. A 1:1000 dilution of Avidin-D-HRP was then added and incubated for 30 minutes at RT. Plates were then washed four times in PBS + 0.5% Tween-20. TMB with peroxide was then added, and the reaction was stopped after 15 minutes with 2N H_2SO_4, and read at OD450nm.

To measure plasma levels of Fgl2, the Fgl2 ELISA kit (BioLegend) was followed according to the manufacturer's instructions.

Lymphocyte isolation from peripheral organs—Prior to organ harvesting, the heart and portal vein were perfused with 10 mL cold PBS. Livers were homogenized manually and filtered, and then spun lightly at 300rpm to pellet the hepatocytes. The supernatant was resuspended in a 40% percoll solution and overlaid on 60% percoll, and then spun at 2000rpm for 20 minutes. The buffy coat was isolated, washed, and stained with antibodies for flow cytometry. Lungs were chopped and digested for 1 hour at 37°C with 1.5mg/mL Collagenase (type 1A, Sigma-Aldrich, C2654) and 0.75mg/mL hyaluronidase (type 1, Sigma-Aldrich,) in DMEM + 10% FBS. Digested lungs were then homogenized, filtered, washed, and stained with antibodies for flow cytometry. Heart and kidney were chopped and digested with 0.5mg/mL Collagenase D (Sigma- Aldrich) in HBSS (with calcium and magnesium) with 5% FBS, 10mM HEPES, and 2mM EDTA for 40 minutes at 37°C with shaking (200rpm). The digested kidney and heart were then homogenized, filtered, washed, and stained with antibodies for flow cytometry. Skin grafts were cleaned and defatted, chopped, and digested with 2mg/mL Collagenase P (Sigma-Aldrich) in HBSS (with calcium and magnesium) for 30 minutes at 37°C. Digested lungs were then homogenized, filtered, washed, and stained with antibodies for flow cytometry.

Flow cytometry, transcription factor staining, and intracellular cytokine staining—Spleens were processed into single cell suspensions and stained according to manufacturer's instructions with CD3e- BV650 (BD Biosciences), biotinylated CD16/CD32 (2.4G2, BD Biosciences), biotinylated isotype control (IgG2b κ isotype, BD Biosciences), and CD4-PacBlue, CD8- BV785, CD19-BV510, CD11c- FITC, CD44- APC-Cy7, CD62L-PE-Cy7,Thy1.1- PerCP, CD45.1- BV605, CD45.2- PE-Dazzle, CD40- FITC, 2B4-PE, CD69- BV711, and streptavidin-APC (all from BioLegend). For Fgl2 staining, anti-Fgl2 (clone 6D9, Abnova) was conjugated to PE using an R-PE conjugation kit according to manufacturer's instructions (Novus, 703–0010). For transcription factor staining, cells were permeabilized using a FoxP3/transcription factor kit (Invitrogen) and stained with Eomes-PE and Tbet- BV421 (BioLegend). For active caspase 3/7 and 7-AAD staining, the caspase 3/7 kit (Thermofisher) was followed according to manufacturer's instructions. For cytokine staining, splenocytes were ex vivo stimulated at 37°C with 30nm $OVA_{257–264}$ (SIINFEKL) peptide and 10ug/mL GolgiPlug (BD Biosciences). After 4 hours, cells were processed and stained using an intracellular cytokine staining kit (BD Biosciences) according to manufacturer's instructions with TNF- PE-Cy7, IFNγ- Alexafluor700, and IL-2- BV421 (all from BioLegend). Samples without peptide were analyzed for unstimulated controls. All flow cytometry samples were acquired on an LSR II flow cytometer (BD Biosciences) and data were analyzed using FlowJo (Tree Star, San Carlos, CA) and Prism (GraphPad Software). Sorting was performed on an ARIAII instrument (BD Biosciences). Absolute cell numbers were calculated using CountBright Beads (Life Technologies) according to the manufacturer's instructions.

In vitro stimulation of WT and Fcgr2b$^{-/-}$ OT-I T cells with Fgl2—5×10^6 splenocytes from WT or *Fcgr2b*$^{-/-}$ OT-I transgenic mice were stimulated for 48 hours with

SIINFEKL peptide. Cells were further stimulated for another 24 hours in the presence or absence of 0.1 or 1.0ug/mL soluble Fgl2 (R&D Systems). Cells were then harvested and caspase 3/7 and 7-AAD (Thermofisher) was assessed via flow cytometry.

PBMC isolation for flow cytometry phenotyping of human CD8$^+$ T cells and sorting for qPCR—Patients undergoing renal transplantation at Emory University Hospital between the years 2009 and 2015, as well as normal healthy controls, were enrolled in an immune monitoring protocol approved by Emory University's Institutional Review Board (IRB #00046593) after informed consent was obtained. Patient samples for this study were acquired prior to transplantation (baseline). PBMCs were purified from peripheral blood samples via density gradient centrifugation (cell preparation tubes, BD Pharmingen) and cryopreserved at −80 degrees C at the Emory Transplant Center Biorepository. For phenotyping of isolated PBMCs, the following antibodies were used: CD14/CD19-V500 (BD Pharmingen), CD8-BV785 (BD Pharmingen), CD4-APC-H7 (BD Pharmingen), and anti-CD32-PE (clone FUN-2, BioLegend). For FACS sorting, standard extracellular staining was performed on PBMCs using the following fluorophore-labeled antibodies: BV510-CD19 (BD Pharmingen), BV510-CD14 (BD Pharmingen), CD3-PerCP-Cy5.5 (BD Pharmingen), CD8-BV711 (BD Pharmingen), and CD4-V450 (BD Pharmingen). Following FACS sorting of CD19$^-$CD14$^-$CD3$^+$CD4$^-$CD8$^+$ T cells, RNA was purified using the RNeasy Plus Micro Kit (Qiagen cat. #74034) and then converted to cDNA using the High Capacity cDNA reverse transcription kit (Thermo Fisher cat. #4368814). cDNA was then used as template in a qPCR reaction with PCR Taqman probes for *FCGR2B* (Thermo Fisher, Hs00269610_m1, cat. # 4448892) and *GAPDH* (Thermo Fisher, Hs02786624_g1, cat. # 4331182). Quantitative RT-PCR was performed using the QuantStudio Flex Systems (Thermo Fisher Scientific). ΔΔCT values were determined by normalizing to *GAPDH* and normalizing to the CD4$^+$ ΔCT values. Relative mRNA expression of *FCGR2B* were determined using the $2^{-\Delta\Delta CT}$ method.

viSNE analysis—viSNE (visual high-dimensional single-cell data analysis based on the t-Distributed Stochastic Neighbor Embedding (t-SNE) algorithm) allows visualization of multi-dimensional data as a 2D scatter plot (Amir el et al., 2013). viSNE was performed in cytobank (Cytobank, Santa Clara, CA). FCS files of CD8$^+$ T cells on day 14 post transplantation with OVA-expressing skin were imported into cytobank and viSNE was run using default parameters (iterations= 1000, perplexity= 30, and theta=0.5). The median fluorescent intensity for each marker is displayed on the plot, with a scale representing the range of fluorescent intensity (high-red, low-blue) on the left-hand side. From the Thy1.1 and FcγRIIB plots, Thy1.1$^+$ FcγRIIB$^+$ and Thy1.1$^+$ FcγRIIB$^-$ cells were gated on, and MFIs of those cell populations were extracted for 2B4, CD40, CD69, and CD44.

RNA-seq—10^6 antigen-specific OT-I T cells were adoptively transferred 24hrs prior to skin transplantation with OVA-expressing skin. On day 14 post grafting, lymphocytes were ficolled or enriched in CD8$^+$ T cells using the MACS CD8$^+$ negative selection isolation kit (Miltenyi Biotech, 130-104-075). 1000 FcγRIIB$^+$ and FcγRIIB$^-$ CD44^{hi}Thy1.1$^+$CD8$^+$ T cells from the spleen were then isolated by FACS on an ARIAII instrument (BD Biosciences). Total RNA was purified using the Quick-RNA MicroPrep Kit (Zymo

Research) and used as input for the SMART-seq v4 cDNA synthesis kit (Takara). Final libraries were constructed using 200 pg of cDNA as input for the NexteraXT kit with the NexteraXT indexing primers (Illumina). Libraries were quality checked on an Agilent Bioanalyzer, pooled at an equimolar ratio and sequenced on a NextSeq500 using 75 bp paired-end chemistry. Raw sequencing reads were mapped to the mm9 genome using TopHat2 (Kim et al., 2013) and the UCSC mm9 Known Gene reference transcript database (Hsu et al., 2006). For each sample, reads that overlapped exons of unique ENTREZ genes were annotated using the GenomicRanges (v1.22.4) package in R/Bioconductor. Genes with less than 3 reads per million in at least 3 samples were removed and edgeR (Robinson et al., 2010) was used to find significantly differentially expressed genes between FcγRIIB^{+} and FcγRIIB^{-} OT-I T cells. Genes with an FDR < 0.05 were termed significant. For GSEA, all detected genes were ranked by multiplying the sign of the fold change (+ or −) by the -log10 of the *P*-value. The resulting list was used in a GSEA PreRanked analysis. All sequencing data is available from the NCBI Gene Expression Omnibus (GEO) under accession GSE118439.

Microarray Analysis of Transplant Patient PBMC—RNA samples were processed and hybridized to a human HT HG-U133 Plus PM BeadChip gene chip (Affymetrix, Santa Clara, CA). Arrays were processed at Scripps (La Jolla, CA) and raw expression data were obtained. The data were log transformed and RMA normalized. Differential expression between stable and rejection patients was defined with an absolute fold change of at least 1.5, and a significant change in expression by limma (linear models of microarray data, Bioconductor (Gentleman et al., 2004) implementation) after correction for multiple-hypothesis testing. Genes with multiple probes were collapsed to keep probes with the highest average expression within differentially expressed genes. CellCODE (Chikina et al., 2015) analysis was applied to the samples before Tac withdrawal (6 months post-transplant) using the IRIS dataset (Abbas et al., 2009) to obtain the tag matrix. Average *FCGR2B* mRNA expression in each cell subset was inferred from correlation analysis between the total *FCGR2B* mRNA expression and the surrogate proportion variables (SPVs) obtained with CellCODE in each sample. SPVs were converted into proportions of PBMCs using paired SPV-flow cytometry measurements obtained from similar studies (Chikina et al., 2015). The association of each cell subset with the differences observed between stable and rejection patients were obtained using an interaction model, which included the SPVs, and deriving an interaction F statistic for each cell subset (Chikina et al., 2015).

QUANTIFICATION AND STATISTICAL ANALYSIS

Wilcoxon matched-pairs signed rank tests were performed to compare two groups in the co-transfer experiments or if comparisons were made within the same host animals, and Mann-Whitney tests were performed to compare unpaired groups. One-way ANOVA with multiple comparisons was performed when comparing multiple groups, two-way ANOVA with multiple comparisons was performed when comparing multiple groups. Survival data were plotted on Kaplan-Meier curves, and a log-rank (Mantel-Cox) test was performed. All analyses were done using Prism (GraphPad Software). In all legends and figures, mean ± SEM is shown, and *p<0.05, **p<0.01, ***p<0.001, ****p<0.0001.

DATA AND CODE AVAILABILITY

RNAseq data generated in the study have been deposited to NCBI Gene Expression Omnibus (GEO) under accession GSE118439.

Supplementary Material

Refer to Web version on PubMed Central for supplementary material.

Acknowledgements

The authors would like to acknowledge the contributions of the NIAID Clinical Trials in Organ Transplantation Consortium, including CTOT09 investigators Donald E. Hricik (University Hospitals Case Medical Center, Cleveland OH USA), Richard N. Formica (Yale University School of Medicine, New Haven CT USA), Peter Nickerson and David Rush (University of Manitoba, Winnipeg, Manitoba, Canada), Emilio D. Poggio, (Cleveland Clinic, Cleveland OH), Kathryn Tinckam (University of Toronto, Toronto Canada) Suphamai Bunnapradist, Milagros Samaniego-Picota (University of Michigan Medical Center, Ann Arbor MI USA) Daniel C. Brennan (Washington University, St. Louis MO USA) Bernd Schröppel (Icahn School of Medicine at Mount Sinai, NY, NY USA), Osama Gaber (Houston Methodist Hospital, Houston TX and Weil Cornell Medical College, NY, NY USA), Nancy D. Bridges (National Institute of Allergy and Infectious Diseases, National Institutes of Health, Bethesda MD). The arrays on CTOT samples were performed by the late Dr. Dan Salomon, the Scripps Research Institute, La Jolla CA. We also acknowledge Dr. Aaron Rae and the Emory Pediatrics Flow Core, Dr. Jennifer Robertson (Emory University), Ms. Lisa Anderson (Mt. Sinai School of Medicine), and Dr. Marvi Tariq (Emory University) for assistance with flow cytometry, and the NYU Genome Technology Center for Illumina sequencing. The study was funded by NIH awards AI073707 and AI104699 to MLF. The CTOT09 trial was supported by NIH (NIAID) U01 AI63594 awarded to PSH.

References

Abbas AR, Wolslegel K, Seshasayee D, Modrusan Z, and Clark HF (2009). Deconvolution of blood microarray data identifies cellular activation patterns in systemic lupus erythematosus. PLoS One 4, e6098. [PubMed: 19568420]

Alfei F, Kanev K, Hofmann M, Wu M, Ghoneim HE, Roelli P, Utzschneider DT, von Hoesslin M, Cullen JG, Fan Y, et al. (2019). TOX reinforces the phenotype and longevity of exhausted T cells in chronic viral infection. Nature 571, 265–269. [PubMed: 31207605]

Altman MC, Gill MA, Whalen E, Babineau DC, Shao B, Liu AH, Jepson B, Gruchalla RS, O'Connor GT, Pongracic JA, et al. (2019). Transcriptome networks identify mechanisms of viral and nonviral asthma exacerbations in children. Nat Immunol 20, 637–651. [PubMed: 30962590]

Amir el AD, Davis KL, Tadmor MD, Simonds EF, Levine JH, Bendall SC, Shenfeld DK, Krishnaswamy S, Nolan GP, and Pe'er D (2013). viSNE enables visualization of high dimensional single-cell data and reveals phenotypic heterogeneity of leukemia. Nat Biotechnol 31, 545–552. [PubMed: 23685480]

Anderson CL, and Grey HM (1974). Receptors for aggregated IgG on mouse lymphocytes: their presence on thymocytes, thymus-derived, and bone marrow-derived lymphocytes. J Exp Med 139, 1175–1188. [PubMed: 4132993]

Barnden MJ, Allison J, Heath WR, and Carbone FR (1998). Defective TCR expression in transgenic mice constructed using cDNA-based alpha- and beta-chain genes under the control of heterologous regulatory elements. Immunol Cell Biol 76, 34–40. [PubMed: 9553774]

Bolland S, Pearse RN, Kurosaki T, and Ravetch JV (1998). SHIP modulates immune receptor responses by regulating membrane association of Btk. Immunity 8, 509–516. [PubMed: 9586640]

Boross P, Arandhara VL, Martin-Ramirez J, Santiago-Raber ML, Carlucci F, Flierman R, van der Kaa J, Breukel C, Claassens JW, Camps M, et al. (2011). The inhibiting Fc receptor for IgG, FcgammaRIIB, is a modifier of autoimmune susceptibility. J Immunol 187, 1304–1313. [PubMed: 21724994]

Brown DM, Fisher TL, Wei C, Frelinger JG, and Lord EM (2001). Tumours can act as adjuvants for humoral immunity. Immunology 102, 486–497. [PubMed: 11328383]

Chikina M, Zaslavsky E, and Sealfon SC (2015). CellCODE: a robust latent variable approach to differential expression analysis for heterogeneous cell populations. Bioinformatics 31, 1584–1591. [PubMed: 25583121]

Ehst BD, Ingulli E, and Jenkins MK (2003). Development of a novel transgenic mouse for the study of interactions between CD4 and CD8 T cells during graft rejection. Am J Transplant 3, 1355–1362. [PubMed: 14525595]

Foerster K, Helmy A, Zhu Y, Khattar R, Adeyi OA, Wong KM, Shalev I, Clark DA, Wong PY, Heathcote EJ, et al. (2010). The novel immunoregulatory molecule FGL2: a potential biomarker for severity of chronic hepatitis C virus infection. J Hepatol 53, 608–615. [PubMed: 20615566]

Gentleman RC, Carey VJ, Bates DM, Bolstad B, Dettling M, Dudoit S, Ellis B, Gautier L, Ge Y, Gentry J, et al. (2004). Bioconductor: open software development for computational biology and bioinformatics. Genome Biol 5, R80. [PubMed: 15461798]

Hartmann BM, Albrecht RA, Zaslavsky E, Nudelman G, Pincas H, Marjanovic N, Schotsaert M, Martinez-Romero C, Fenutria R, Ingram JP, et al. (2017). Pandemic H1N1 influenza A viruses suppress immunogenic RIPK3-driven dendritic cell death. Nat Commun 8, 1931. [PubMed: 29203926]

Hogquist KA, Jameson SC, Heath WR, Howard JL, Bevan MJ, and Carbone FR (1994). T cell receptor antagonist peptides induce positive selection. Cell 76, 17–27. [PubMed: 8287475]

Hricik DE, Formica RN, Nickerson P, Rush D, Fairchild RL, Poggio ED, Gibson IW, Wiebe C, Tinckam K, Bunnapradist S, et al. (2015). Adverse Outcomes of Tacrolimus Withdrawal in Immune-Quiescent Kidney Transplant Recipients. J Am Soc Nephrol 26, 3114–3122. [PubMed: 25925687]

Hsu F, Kent WJ, Clawson H, Kuhn RM, Diekhans M, and Haussler D (2006). The UCSC Known Genes. Bioinformatics 22, 1036–1046. [PubMed: 16500937]

Joller N, Lozano E, Burkett PR, Patel B, Xiao S, Zhu C, Xia J, Tan TG, Sefik E, Yajnik V, et al. (2014). Treg cells expressing the coinhibitory molecule TIGIT selectively inhibit proinflammatory Th1 and Th17 cell responses. Immunity 40, 569–581. [PubMed: 24745333]

Kaech SM, and Cui W (2012). Transcriptional control of effector and memory CD8+ T cell differentiation. Nat Rev Immunol 12, 749–761. [PubMed: 23080391]

Kim D, Pertea G, Trapnell C, Pimentel H, Kelley R, and Salzberg SL (2013). TopHat2: accurate alignment of transcriptomes in the presence of insertions, deletions and gene fusions. Genome Biol 14, R36. [PubMed: 23618408]

Latha K, Yan J, Yang Y, Gressot LV, Kong LY, Manyam G, Ezhilarasan R, Wang Q, Sulman EP, Eric Davis R, et al. (2019). The Role of Fibrinogen-Like Protein 2 on Immunosuppression and Malignant Progression in Glioma. J Natl Cancer Inst 111, 292–300. [PubMed: 29947810]

Lee HJ, Georgiadou A, Walther M, Nwakanma D, Stewart LB, Levin M, Otto TD, Conway DJ, Coin LJ, and Cunnington AJ (2018). Integrated pathogen load and dual transcriptome analysis of systemic host-pathogen interactions in severe malaria. Sci Transl Med 10.

Li F, Smith P, and Ravetch JV (2014). Inhibitory Fcgamma receptor is required for the maintenance of tolerance through distinct mechanisms. J Immunol 192, 3021–3028. [PubMed: 24563255]

Liu C, Chikina M, Deshpande R, Menk AV, Wang T, Tabib T, Brunazzi EA, Vignali KM, Sun M, Stolz DB, et al. (2019). Treg Cells Promote the SREBP1-Dependent Metabolic Fitness of Tumor-Promoting Macrophages via Repression of CD8(+) T Cell-Derived Interferon-gamma. Immunity 51, 381–397 e386. [PubMed: 31350177]

Liu H, Shalev I, Manuel J, He W, Leung E, Crookshank J, Liu MF, Diao J, Cattral M, Clark DA, et al. (2008). The FGL2-FcgammaRIIB pathway: a novel mechanism leading to immunosuppression. Eur J Immunol 38, 3114–3126. [PubMed: 18991288]

Marsden PA, Ning Q, Fung LS, Luo X, Chen Y, Mendicino M, Ghanekar A, Scott JA, Miller T, Chan CW, et al. (2003). The Fgl2/fibroleukin prothrombinase contributes to immunologically mediated thrombosis in experimental and human viral hepatitis. J Clin Invest 112, 58–66. [PubMed: 12840059]

Muramatsu M, Kinoshita K, Fagarasan S, Yamada S, Shinkai Y, and Honjo T (2000). Class switch recombination and hypermutation require activation-induced cytidine deaminase (AID), a potential RNA editing enzyme. Cell 102, 553–563. [PubMed: 11007474]

Nimmerjahn F, and Ravetch JV (2008). Fcgamma receptors as regulators of immune responses. Nat Rev Immunol 8, 34–47. [PubMed: 18064051]

Ono M, Bolland S, Tempst P, and Ravetch JV (1996). Role of the inositol phosphatase SHIP in negative regulation of the immune system by the receptor Fc(gamma)RIIB. Nature 383, 263–266. [PubMed: 8805703]

Pearse R, Kawabe T, Boiland S, Guinamard R, Kurosaki T, and Ravetch J (1999). SHIP recruitment attentuates FcgRIIB- induced B cell apoptosis. Immunity 10, 753–760. [PubMed: 10403650]

Ravetch JV, Luster AD, Weinshank R, Kochan J, Pavlovec A, Portnoy DA, Hulmes J, Pan YC, and Unkeless JC (1986). Structural heterogeneity and functional domains of murine immunoglobulin G Fc receptors. Science 234, 718–725. [PubMed: 2946078]

Robbiani DF, Bothmer A, Callen E, Reina-San-Martin B, Dorsett Y, Difilippantonio S, Bolland DJ, Chen HT, Corcoran AE, Nussenzweig A, and Nussenzweig MC (2008). AID is required for the chromosomal breaks in c-myc that lead to c-myc/IgH translocations. Cell 135, 1028–1038. [PubMed: 19070574]

Robinson MD, McCarthy DJ, and Smyth GK (2010). edgeR: a Bioconductor package for differential expression analysis of digital gene expression data. Bioinformatics 26, 139–140. [PubMed: 19910308]

Smith KG, and Clatworthy MR (2010). FcgammaRIIB in autoimmunity and infection: evolutionary and therapeutic implications. Nat Rev Immunol 10, 328–343. [PubMed: 20414206]

Starbeck-Miller GR, Badovinac VP, Barber DL, and Harty JT (2014). Cutting edge: Expression of FcgammaRIIB tempers memory CD8 T cell function in vivo. J Immunol 192, 35–39. [PubMed: 24285839]

Stout RD, and Herzenberg LA (1975). The Fc receptor on thymus-derived lymphocytes. I. Detection of a subpopulation of murine T lymphocytes bearing the Fc receptor. J Exp Med 142, 611–621. [PubMed: 1100762]

Takai T, Ono M, Hikida M, Ohmori H, and Ravetch JV (1996). Augmented humoral and anaphylactic responses in Fc gamma RII-deficient mice. Nature 379, 346–349. [PubMed: 8552190]

Tang M, Cao X, Li P, Zhang K, Li Y, Zheng QY, Li GQ, Chen J, Xu GL, and Zhang KQ (2017). Increased expression of Fibrinogen-Like Protein 2 is associated with poor prognosis in patients with clear cell renal cell carcinoma. Sci Rep 7, 12676. [PubMed: 28978925]

Trambley J, Bingaman AW, Lin A, Elwood ET, Waitze SY, Ha J, Durham MM, Corbascio M, Cowan SR, Pearson TC, and Larsen CP (1999). Asialo GM1(+) CD8(+) T cells play a critical role in costimulation blockade-resistant allograft rejection. J Clin Invest 104, 1715–1722. [PubMed: 10606625]

Williams EL, Tutt AL, French RR, Chan HT, Lau B, Penfold CA, Mockridge CI, Roghanian A, Cox KL, Verbeek JS, et al. (2012). Development and characterisation of monoclonal antibodies specific for the murine inhibitory FcgammaRIIB (CD32B). Eur J Immunol 42, 2109–2120. [PubMed: 22760702]

Wirth TC, Xue HH, Rai D, Sabel JT, Bair T, Harty JT, and Badovinac VP (2010). Repetitive antigen stimulation induces stepwise transcriptome diversification but preserves a core signature of memory CD8(+) T cell differentiation. Immunity 33, 128–140. [PubMed: 20619696]

Yan J, Kong LY, Hu J, Gabrusiewicz K, Dibra D, Xia X, Heimberger AB, and Li S (2015). FGL2 as a Multimodality Regulator of Tumor-Mediated Immune Suppression and Therapeutic Target in Gliomas. J Natl Cancer Inst 107.

Yan J, Zhao Q, Gabrusiewicz K, Kong LY, Xia X, Wang J, Ott M, Xu J, Davis RE, Huo L, et al. (2019). FGL2 promotes tumor progression in the CNS by suppressing CD103(+) dendritic cell differentiation. Nat Commun 10, 448. [PubMed: 30683885]

Yoshida TO, and Andersson B (1972). Evidence for a receptor recognizing antigen complexed immunoglobulin on the surface of activated mouse thymus lymphocytes. Scand J Immunol 1, 401–408. [PubMed: 4544080]

Zhu Y, Zhang L, Zha H, Yang F, Hu C, Chen L, Guo B, and Zhu B (2017). Stroma-derived Fibrinogen-like Protein 2 Activates Cancer-associated Fibroblasts to Promote Tumor Growth in Lung Cancer. Int J Biol Sci 13, 804–814. [PubMed: 28656005]

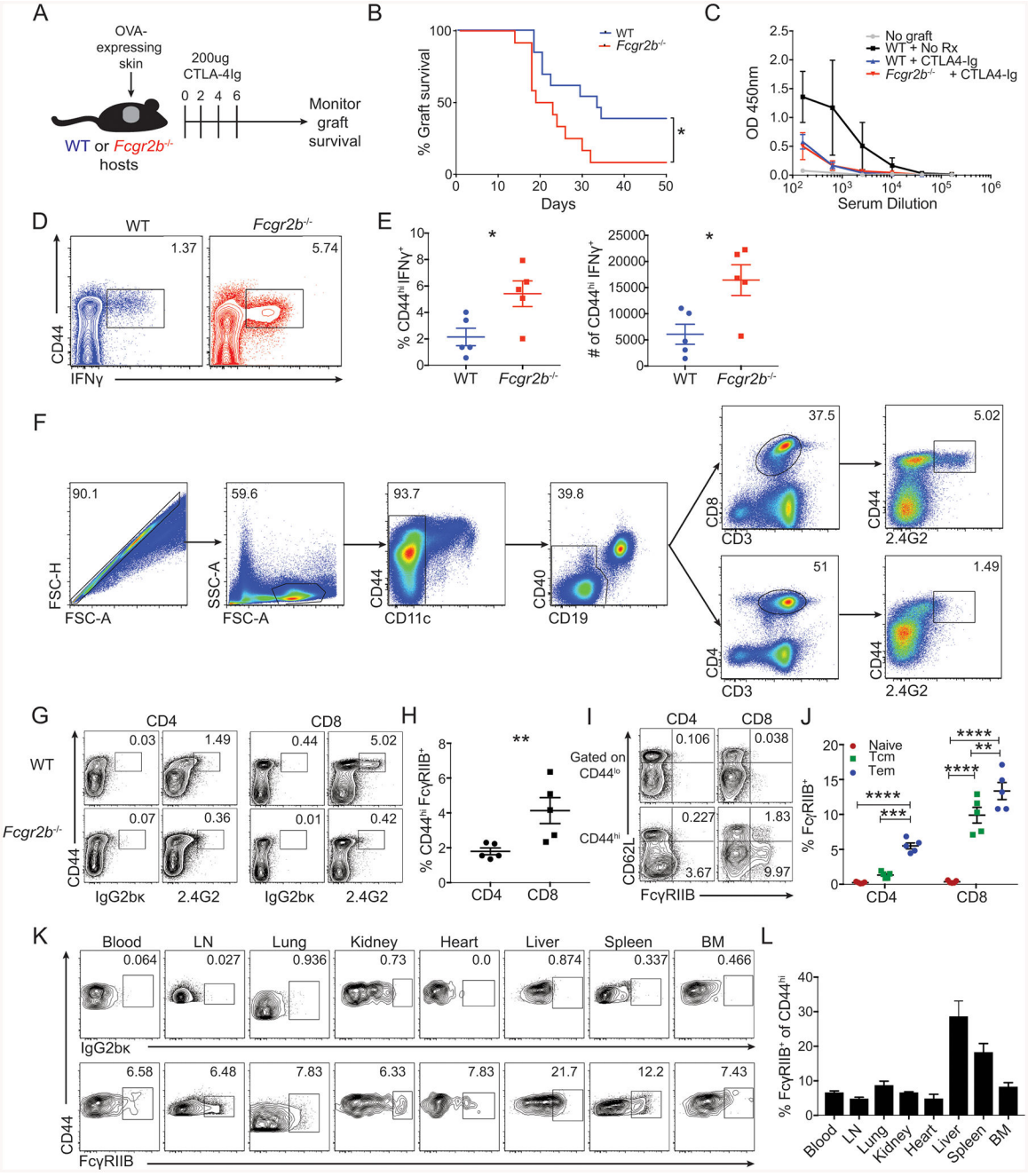

Figure 1: FcγRIIB is expressed on a subset of effector-memory CD8$^+$ T cells.

(A-E) A: Schematic of experimental design for panels B-E: WT or *Fcgr2b*$^{-/-}$ animals (Jackson- B6;129S-Fcgr2b^{tm1Ttk}/J (Takai et al., 1996)) were grafted with OVA-expressing skin and treated with 250ug CTLA-4Ig on days 0, 2, 4 and 6.

B. Summary of graft survival (Log-rank (Mantel-Cox) test, p= 0.0124)). Pooled data from two independent experiments, n=7–10 mice per group.

C. Readout at OD450nm of an anti-OVA total IgG ELISA from serum collected on day 13 post grafting. Representative data from two independent experiments, n=4–5 mice per group.

D. Mice were sacrificed at day 14 post grafting and splenocytes were analyzed by flow cytometry for the frequency of $CD44^{hi}IFN\gamma^{+}$ of $CD8^{+}$ T cells in WT and *Fcgr2b*$^{-/-}$ animals (Jackson- B6;129S-Fcgr2b^{tm1Ttk}/J). Representative flow plots are shown.

E. Mice were sacrificed at day 14 post grafting and splenocytes were analyzed by flow cytometry for the frequency and number of $CD44^{hi}IFN\gamma^{+}$ $CD8^{+}$ T cells in WT and *Fcgr2b*$^{-/-}$ shown in D. Representative data from two independent experiments, n=5 mice per group, ± SEM. Mann-Whitney test, *p<0.05).

(F-J) Splenocytes from mice aged 6 months or older were analyzed by flow cytometry for T cell expression of FcγRIIB through staining with the monoclonal antibody anti-CD16/CD32 (clone 2.4G2). Representative data from two independent experiments, n=5 mice per group.

F: Gating strategy for excluding $CD11c^{+}$ and $CD19^{+}$ cells and gating on $CD3^{+}CD8^{+}$ or $CD3^{+}CD4^{+}$ double-positive T cells in the spleen. Gates were drawn for 2.4G2 using an isotype control.

G: Representative flow cytometric plots of the expression of 2.4G2 (or isotype control IgG2bκ) for $CD4^{+}$ and $CD8^{+}$ populations in the spleen of WT and *Fcgr2b*$^{-/-}$ animals (Jackson- B6;129S-Fcgr2b^{tm1Ttk}/J).

H: The frequency of $CD44^{hi}$ $Fc\gamma RIIB^{+}$ cells of the $CD4^{+}$ and $CD8^{+}$ T cell compartments in WT animals. Summary data ± SEM of G is shown. Mann-Whitney test, **p<0.01).

I: Representative flow cytometric plots of the expression of 2.4G2 (anti-FcγRIIB) for $CD44^{lo}$ and $CD44^{hi}$ $CD4^{+}$ and $CD8^{+}$ T cells in the spleen. Frequencies are included for $CD44^{lo}CD62L^{+}$ (naïve cells), $CD44^{hi}CD62L^{+}$ (Tcm cells), and $CD44^{hi}CD62L^{lo}$ (Tem cells).

J: The frequency of $2.4G2^{+}$ (anti-FcγRIIB) cells of $CD44^{lo}CD62L^{+}$ (naïve cells), $CD44^{hi}CD62L^{+}$ (Tcm cells), and $CD44^{hi}CD62L^{lo}$ (Tem cells) $CD8^{+}$ T cells. Summary data ± SEM is shown. Two-way ANOVA with multiple comparisons, **p<0.01, ***p<0.001, ****p<0.0001).

(K-L) Naïve B6 hosts were grafted with OVA-expressing skin and sacrificed at day 10. The blood, lymph nodes, lung, kidney, heart, liver, spleen, and bone marrow were harvested and analyzed by flow cytometry. Pooled data from two independent experiments, n=3 mice per group.

K: Representative flow cytometric plots of $CD44^{hi}$ endogenous $CD8^{+}$ T cells from the blood, lymph nodes, lung, kidney, heart, liver, spleen, and bone marrow on day 10. Gates for FcγRIIB were drawn according to binding of the cell-specific population to the isotype control antibody (top row).

L: The frequency of $Fc\gamma RIIB^{+}$ cells of the $CD44^{hi}$ endogenous $CD8^{+}$ T cell population in the blood, lymph nodes, lung, kidney, heart, liver, spleen, and bone marrow on day 10, as shown in K. Summary data ± SEM is shown.

See also Figure S1.

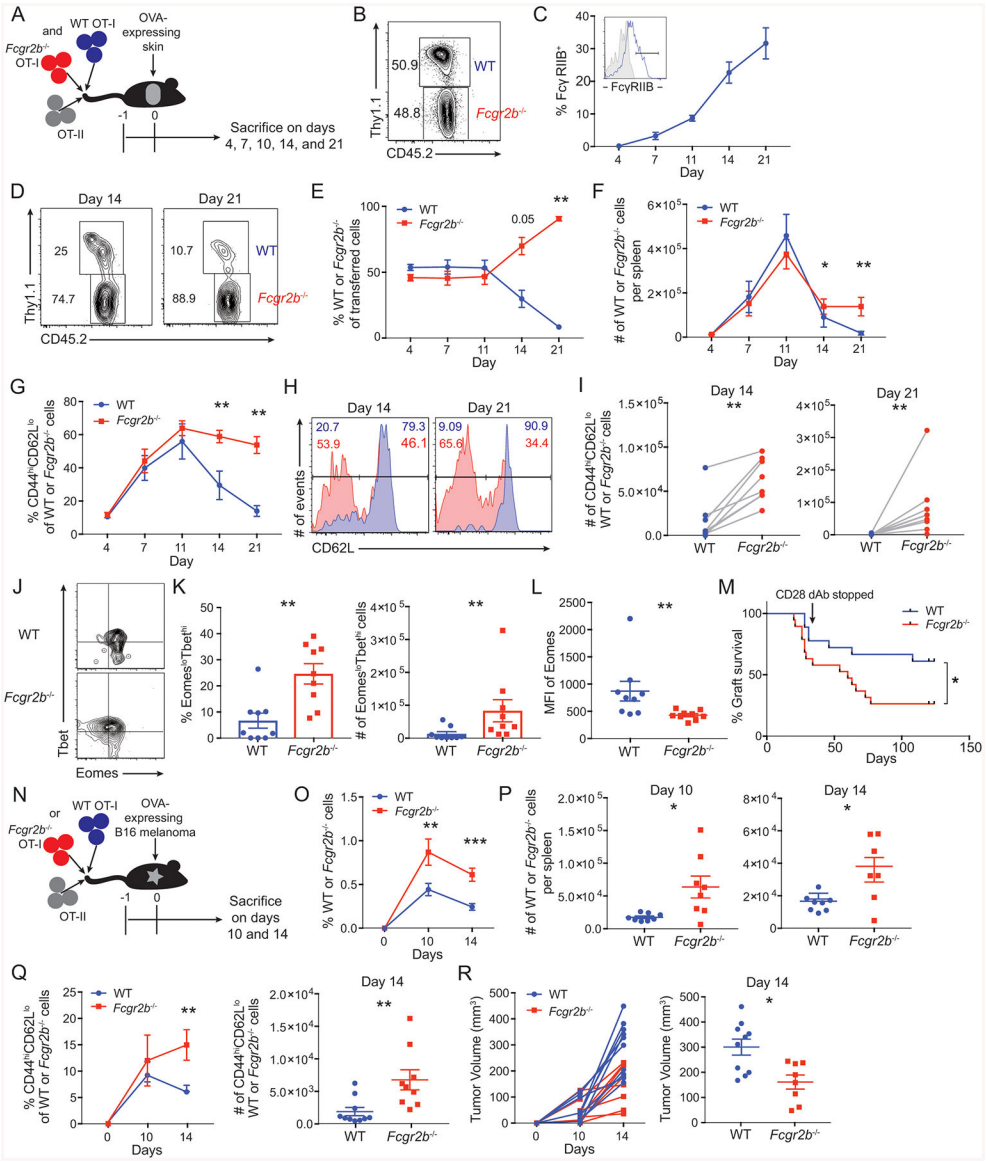

Figure 2: FcγRIIB functions intrinsically on CD8$^+$ T cells to limit T cell responses.

(A-L) A: Schematic of experimental design for panels B-L: 5×10^5 WT Thy1.1$^+$ OT-I T cells, 5×10^5 *Fcgr2b*$^{-/-}$ CD45.2$^+$ OT-I T cells, and 10^6 Thy1.1$^+$ OT-II T cells were harvested from the spleen and mesenteric lymph node and adoptively transferred into congenically marked (CD45.1$^+$, Thy1.2$^+$) naïve mice 24 hours prior to skin transplantation with OVA-expressing skin. Mice were sacrificed at indicated timepoints and splenocytes were analyzed by flow cytometry.

B: Prior to transfer, flow cytometry was performed to determine the ratio of WT to *Fcgr2b*$^{-/-}$ OT-I T cells.

C: FcγRIIB expression on WT OT-I T splenocytes at the indicated timepoints. Inset histograms show gating strategy for FcγRIIB (tinted gray histogram shows isotype control (IgG2bκ)). Summary data ±SEM is shown. Pooled data from 2 independent experiments, n=5 mice per group.

D: Representative flow cytometric plots on day 14 and 21 in the spleen of the ratio of WT to *Fcgr2b*$^{-/-}$ OT-I T cells based on the expression of CD45.2 and Thy1.1.

E: The frequency of WT to *Fcgr2b*$^{-/-}$ OT-I T cells based on expression of CD45.2 and Thy1.1 in the spleen. Summary data ±SEM is shown. Pooled data from 2 independent experiments, n=5 mice per group. Wilcoxon test on individual time points, **p<0.01.

F: The absolute cell number per spleen of WT and *Fcgr2b*$^{-/-}$ OT-I T cells. Summary data ±SEM is shown. Representative data from 2 independent experiments, n=5 mice per group. Wilcoxon test on individual time points, *p<0.05, **p<0.01.

G: The frequency of CD44^{hi}CD62L^{lo} cells of WT or *Fcgr2b*$^{-/-}$ OT-I T cell populations in the spleen. Summary data ±SEM is shown. Pooled data from 2 independent experiments, n=5 mice per group. Wilcoxon test on individual time points, **p<0.01.

H: Flow cytometric plots on days 14 and 21 in the spleen for the expression of CD62L on WT (blue) or *Fcgr2b*$^{-/-}$ (red) OT-I T cells. Representative data from 2 independent experiments, n=5 mice per group.

I: The absolute number per spleen of CD44^{hi}CD62L^{lo} cells of WT or *Fcgr2b*$^{-/-}$ OT-I T cell populations on days 14 and 21. Summary data is shown. Pooled data from 2 independent experiments, n=5 mice per group. Wilcoxon test, p<0.01.

J: Representative flow cytometric plots on day 21 in the spleen of the expression of Tbet and Eomes on WT and *Fcgr2b*$^{-/-}$ OT-I T cell populations at day 21. Representative data from 2 independent experiments, n=5 mice per group.

K: The frequency and absolute cell number per spleen of Eomes^{lo}Tbet^{hi} cells of WT or *Fcgr2b*$^{-/-}$ OT-I T cell populations at day 21. Summary data ±SEM is shown. Pooled data from 2 independent experiments, n=5 mice per group. Wilcoxon test, p<0.01.

L: The geometric mean fluorescent intensity of Eomes on WT or *Fcgr2b*$^{-/-}$ OT-I T cell populations at day 21 in the spleen. Summary data ±SEM is shown. Pooled data from 2 independent experiments, n=5 mice per group. Wilcoxon test, p<0.01.

M: Graft survival data of animals that received either 10^6 WT or *Fcgr2b*$^{-/-}$ OT-I T cells, and 10^6 Thy1.1$^+$ OT-II T cells 24 hours prior to OVA-expressing skin transplantation. Animals were treated with 50ug of CD28 domain antibody on days 0, 2, 4, 6 and every other day thereafter until day 30. Pooled data from 2 independent experiments, n=5 mice per group. Log-rank (Mantel-Cox) test, p= 0.0283.

(N-R) N: Schematic of experimental design for O-R: 10^6 WT Thy1.1$^+$ OT-I T cells or 10^6 *Fcgr2b*$^{-/-}$ CD45.2$^+$ OT-I T cells, and 10^6 Thy1.1$^+$ OT-II T cells were harvested from the spleen and mesenteric lymph nodes and adoptively transferred into congenically marked naïve mice 24 hours prior to inoculation with a B16-melanoma-expressing OVA cell line. Mice were sacrificed at indicated timepoints post tumor inoculation and splenocytes were assessed by flow cytometry.

O: The frequency of WT or *Fcgr2b*$^{-/-}$ OT-I T cells of CD8$^+$ T cells in the spleen. Summary data ± SEM is shown. Pooled data from 2–3 independent experiments, n=3–5 mice per group. Mann-Whitney test for individual timepoints, **p<0.01, ***p<0.001.

P: The absolute cell number per spleen of WT or *Fcgr2b*$^{-/-}$ OT-I T cells on days 10 and 14. Summary data ± SEM is shown. Pooled data from 2–3 independent experiments, n=3–5 mice per group. Mann-Whitney test, *p<0.05.

Q: The frequency and absolute cell number per spleen of CD44^{hi}CD62L^{lo} cells of WT or *Fcgr2b*$^{-/-}$ OT-I T cell populations. Summary data ± SEM is shown. Pooled data from 2–3

independent experiments, n=3–5 mice per group. Mann-Whitney test for individual timepoints, **p<0.01.

R: Mice were sacrificed and tumor volume (measured in mm^3) for each individual mouse that received WT or *Fcgr2b*$^{-/-}$ OT-I T cells was measured. Scatter plot is shown for day 14. Summary data ± SEM is shown. Pooled data from 2–3 independent experiments, n=3–5 mice per group. Mann-Whitney test, *p<0.05.

See also Figure S2.

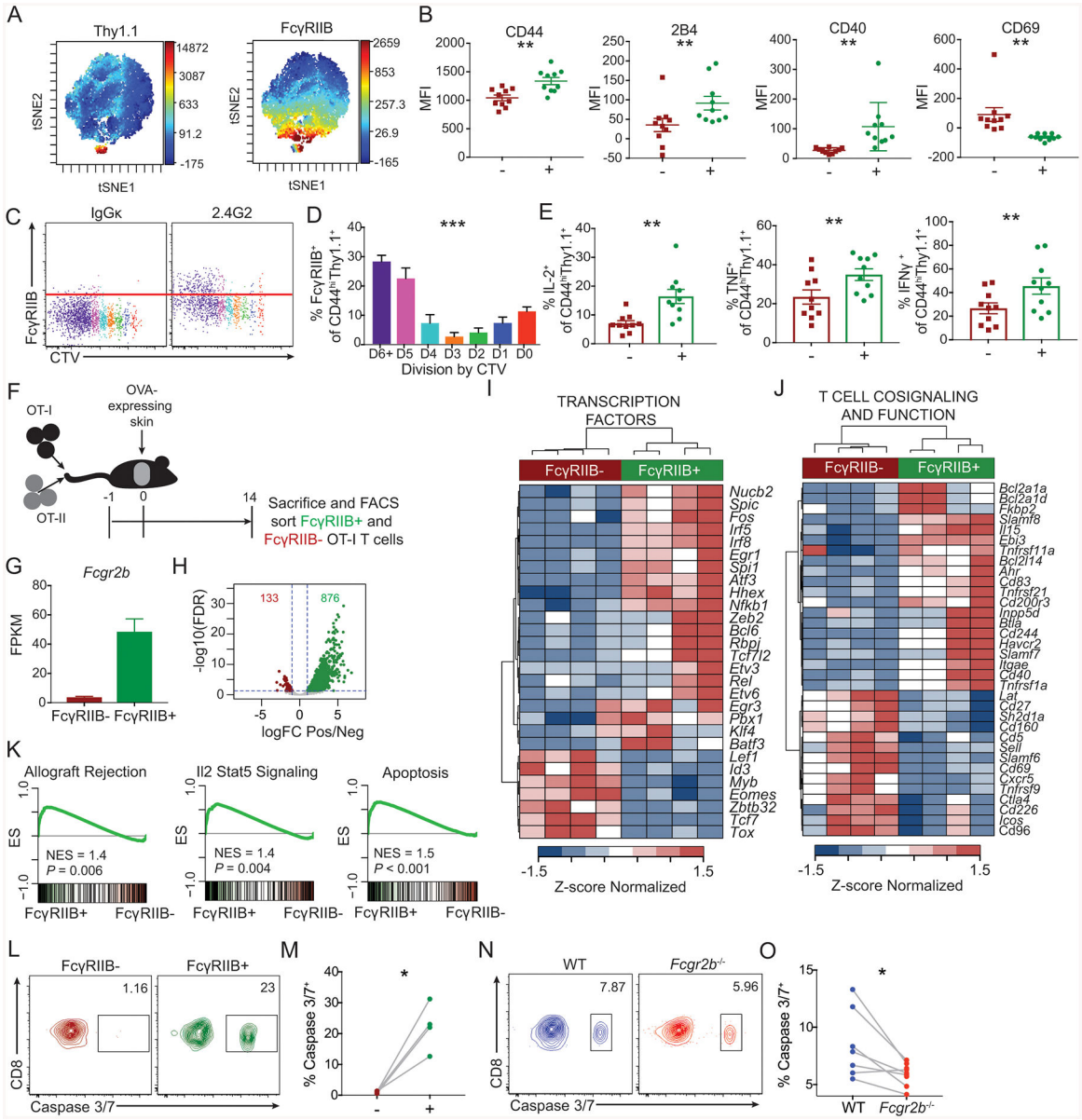

Figure 3: FcγRIIB inhibits highly divided and potent cytokine-producing CD8$^+$ T cell responses by inducing active caspase 3/7 in a cell intrinsic manner.

(A-E)10^6 OT-I and OT-II were harvested from the spleen and mesenteric lymph node and adoptively transferred into naïve hosts 24 hours prior to skin transplantation with OVA-expressing skin. Mice were sacrificed at day 14 post grafting and splenocytes were assessed by flow cytometry.

A: Representative viSNE plots of CD8$^+$ T cells, with high fluorescent intensity displayed as red and low fluorescent intensity displayed as blue for the markers Thy1.1 and FcγRIIB. Representative data from two independent experiments, n=10 mice per group.

B. MFIs were extracted for CD44, 2B4, CD40, and CD69, of the Thy1.1$^+$ FcγRIIB$^+$ and Thy1.1$^+$ FcγRIIB$^-$ viSNE populations. Summary data ±SEM is shown. Representative data from two independent experiments, n=10 mice per group. Wilcoxon test, **p<0.01.

C: Representative flow cytometric plots of CTV by FcγRIIB of OT-I T cells.
D: The frequency of FcγRIIB$^+$ CD44^{hi}Thy1.1$^+$ OT-I T cells by division of CTV. Summary data ±SEM is shown. Representative data from 2 independent experiments, n=4–5 mice per group. One-way ANOVA was performed.
E: The frequencies of IL-2, TNF, and IFN-γ-producing FcγRIIB$^+$ and FcγRIIB$^-$ CD44^{hi}Thy1.1$^+$ OT-I cells following ex vivo stimulation with SIINFEKL peptide. Summary data ±SEM is shown. Pooled data from 2–3 independent experiments, n=5 mice per group. Wilcoxon test, **p<0.01.
(F-K) F: Schematic of experimental design for panels G-K:10^6 Thy1.1$^+$ OT-I and OT-II were harvested from spleen and mesenteric lymph node and adoptively transferred into naïve hosts 24 hours prior to skin transplantation with OVA-expressing skin. On day 14 post grafting, splenocytes were ficolled for lymphocyte isolation, and FcγRIIB$^+$ and FcγRIIB$^-$ CD44^{hi}Thy1.1$^+$ CD8$^+$ T cells were FACS sorted and RNAseq was performed.
G: Fragments per kilobase per million (FPKM) of *Fcgr2b* in the FcγRIIB$^+$ and FcγRIIB$^-$ sorted OT-I T cells.
H: Volcano plot of the differentially expressed genes (DEGs). FDR: False discovery rate, logFC: log2 fold change.
I: Heatmap of DEGs that function as transcription factors.
J: Heatmap of DEGs that contribute to T cell cosignaling and function.
K: GSEA for the indicated HALLMARK gene sets comparing a ranked list of all detected genes between FcγRIIB$^+$ and FcγRIIB$^-$ CD8$^+$ T cells.
(L-M)10^6 OT-I and OT-II were harvested from the spleen and mesenteric lymph node and adoptively transferred into naïve hosts 24 hours prior to skin transplantation with OVA-expressing skin. Mice were sacrificed at day 16 post grafting and splenocytes were assessed by flow cytometry.
L: Representative flow cytometric plots of the expression of active caspase 3/7 of Thy1.1$^+$ CD44^{hi} FcγRIIB$^+$ vs. FcγRIIB$^-$ OT-I T cells of splenic CD8$^+$ T cells on day 16 post grafting. Representative data, n=4 mice per group.
M: The frequency of active caspase 3/7$^+$ cells of Thy1.1$^+$ CD44^{hi} FcγRIIB$^+$ vs. FcγRIIB$^-$ OT-I T cells of splenic CD8$^+$ T cells as shown in K. Summary data are shown, n=4 mice per group. Wilcoxon test, *p<0.05.
(N-O) 5×10^5 WT Thy1.1$^+$ OT-I T cells, 5×10^5 *Fcgr2b*$^{-/-}$ CD45.2$^+$ OT-I T cells, and 10^6 Thy1.1$^+$ OT-II T cells were harvested from the spleen and mesenteric lymph nodes and adoptively transferred into congenically marked (CD45.1) naïve mice 24 hours prior to skin transplantation with OVA-expressing skin. Mice were sacrificed at day 16 post grafting and splenocytes were assessed by flow cytometry.
N: Representative flow cytometric plots of the expression of active caspase 3/7 of Thy1.1$^+$ CD44^{hi} WT and CD45.2$^+$ CD44^{hi} *Fcgr2b*$^{-/-}$ OT-I T cells of splenic CD8$^+$ T cells on day 16 post grafting. Representative data from two independent experiments, n=3–4 mice per group.
O: The frequency of active caspase 3/7$^+$ cells of Thy1.1$^+$ CD44^{hi} WT and CD45.2$^+$ CD44^{hi} *Fcgr2b*$^{-/-}$ OT-I T cells of splenic CD8$^+$ T cells as shown in N. Summary data are shown. Pooled data from two independent experiments, n=3–4 mice per group. Wilcoxon test, *p<0.05.
See also Figure S3.

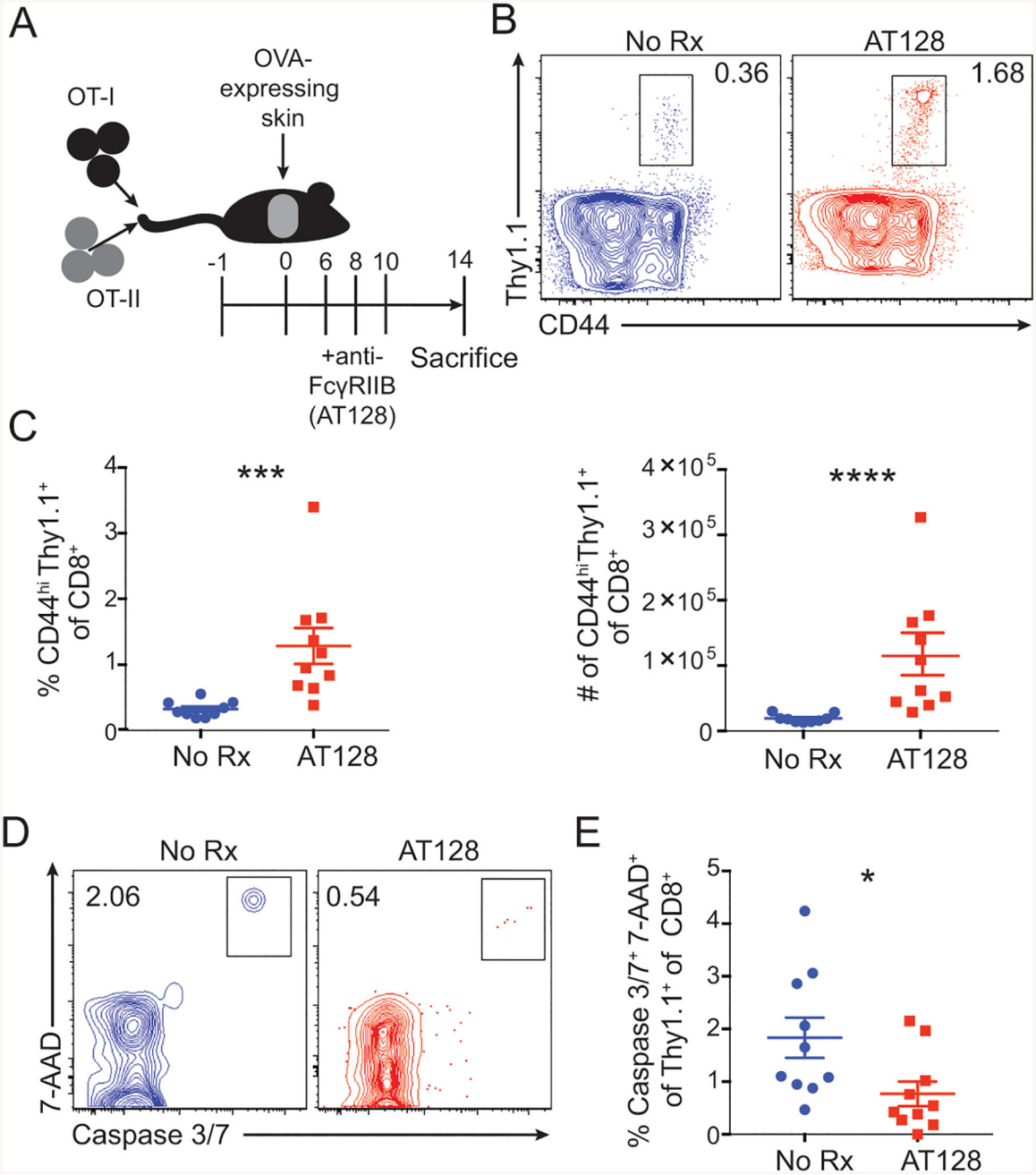

Figure 4: Immunotherapy with anti-FcγRIIB functions to augment CD8$^+$ T cell responses in vivo.

(A-E) A: Schematic of experimental design for panels B-E: 10^6 Thy1.1$^+$ OT-I and OT-II were harvested from spleen and mesenteric lymph node and adoptively transferred 24 hours prior to skin grafting with OVA-expressing skin. Animals were treated with 250ug of the anti-FcγRIIB monoclonal antibody (clone AT-128) on days 6, 8, and 10 post grafting, and splenocytes were analyzed by flow cytometry at day 14.

B: Representative flow cytometric plots of $CD44^{hi}Thy1.1^{+}$ OT-I T cells of splenic $CD8^{+}$ T cells isolated from untreated and AT-128-treated mice. Representative data from 2 independent experiments, n=5 per group.

C: The frequency and absolute cell number of $CD44^{hi}$ $Thy1.1^{+}$ $CD8^{+}$ OT-I T cells of splenic $CD8^{+}$ T cells isolated from untreated and AT-128-treated mice. Summary data ±SEM are shown. Pooled data from 2 independent experiments, n=5 per group. Mann-Whitney test, ***p<0.001.

D: Representative flow cytometric plots of caspase 3/7 and 7-AAD double-positive cells among $CD44^{hi}$ $Thy1.1^{+}$ OT-I T cells of splenic $CD8^{+}$ T cells from untreated and AT-128-treated mice. Representative data from 2 independent experiments, n=5 per group.

E: The frequency of caspase $3/7^{+}$ $7\text{-}AAD^{+}$ cells among the $CD44^{hi}$ $Thy1.1^{+}$ OT-I T cells of the splenic $CD8^{+}$ T cells of untreated and AT-128-treated treated mice. Summary data ±SEM are shown. Pooled data from 2 independent experiments, n=5 per group. Mann-Whitney test, *p<0.05.

See also Figure S4.

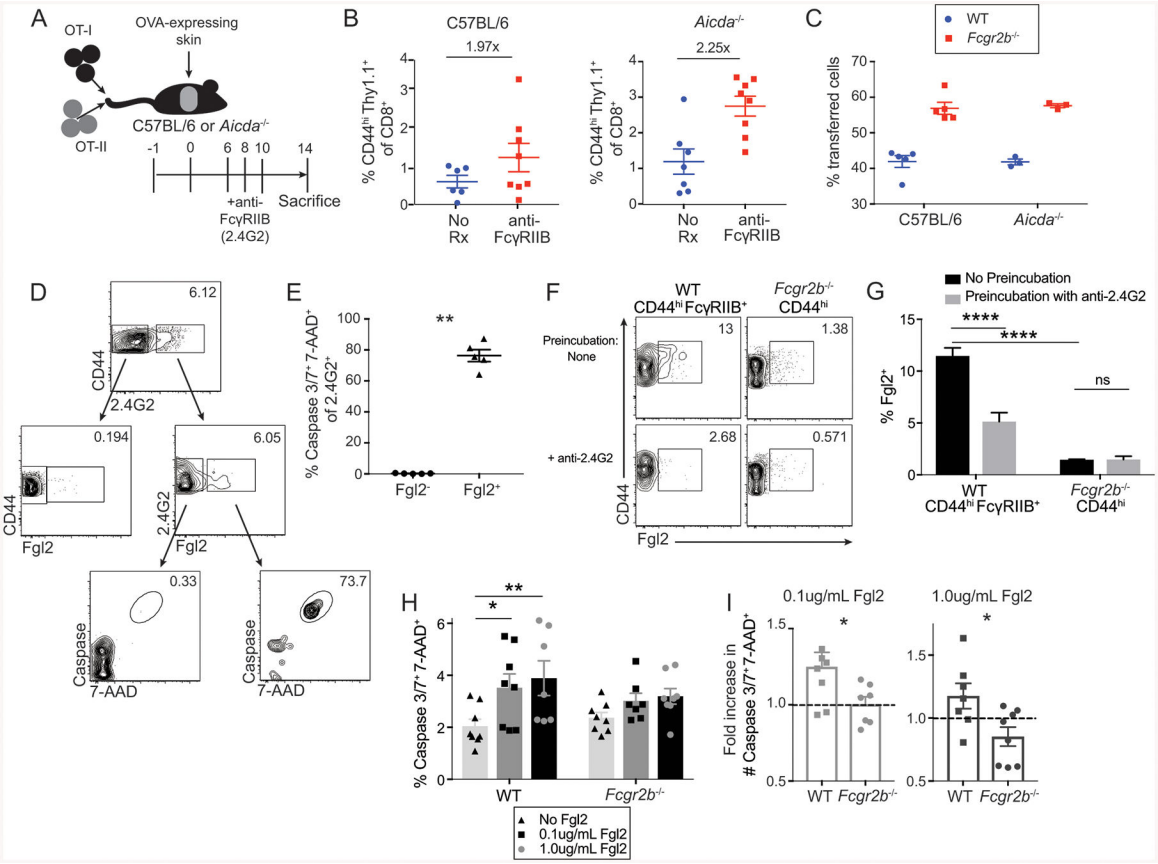

Figure 5: FcγRIIB requires ligation with Fgl2, and not endogenous antibodies, for induction of apoptosis.

(A-B) A: Schematic of experimental design for panel B: 10^6 Thy1.1$^+$ OT-I and OT-II were harvested from spleen and mesenteric lymph node and adoptively transferred into C57BL/6 or *Aicda*$^{-/-}$ animals 24 hours prior to skin grafting with OVA-expressing skin. Animals were treated with 250ug of the monoclonal antibody anti-FcγRIIB (clone 2.4G2) on days 6, 8, and 10 post grafting, and splenocytes were analyzed at day 14.

B: The frequency of CD44^{hi} Thy1.1$^+$ OT-I T cells of splenic CD8$^+$ T cells in C57BL/6 and *Aicda*$^{-/-}$ recipients. Summary data ±SEM are shown. Pooled data from 2–3 independent experiments, n=3–5 per group.

C: 5×10^5 WT Thy1.1$^+$, 5×10^5 *Fcgr2b*$^{-/-}$ Thy1.1$^+$ Thy1.2$^+$ OT-I T cells, and 10^6 OT-II T cells were harvested from the spleen and mesenteric lymph nodes and adoptively transferred into C57BL/6 and *Aicda*$^{-/-}$ recipients 24 hours prior to skin transplantation with OVA-expressing skin. Frequencies of WT vs *Fcgr2b*$^{-/-}$ T cells were assessed on day 21 post-transplant in the draining lymph node (axial and brachial). Summary data ±SEM are shown. Representative data from 2 independent experiments, n=5 mice per group

D: WT B6 mice received OVA-expressing skin grafts and were sacrificed at day 14. Splenocytes were analyzed via flow cytometry. Bulk CD8$^+$ CD44^{hi} cells were stained for anti-FcγRIIB (clone 2.4G2) and Fgl2. Gating strategy is as follows: CD44^{hi}CD8$^+$ T cells are gated on 2.4G2$^-$ and 2.4G2$^+$ cells. 2.4G2$^-$ and 2.4G2$^+$ cells are then gated for Fgl2.

2.4G2^{+}Fgl2^{-} and 2.4G2^{+}Fgl2^{+} cells are then gated for frequency of caspase 3/7 and 7-AAD double-positive cells.

E: The frequency of caspase 3/7^{+} 7-AAD^{+} cells from the 2.4G2^{+}Fgl2^{-} and 2.4G2^{+}Fgl2^{+} populations gated on in D. Summary data ±SEM are shown, n=5 mice. Mann-Whitney test, **p<0.01.

F: CD44^{hi}FcγRIIB^{+} CD8^{+} T cell splenocytes from naïve WT mice or CD44^{hi} CD8^{+} T cell splenocytes from naïve *Fcgr2b*$^{-/-}$ mice, aged 6 months, were either preincubated with media or anti-FcγRIIB (clone 2.4G2) and then stained with Fgl2. Representative flow cytometric plots of Fgl2 expression is shown, n=4 replicates per group.

G: The frequency of Fgl2^{+} cells from either CD44^{hi} FcγRIIB^{+} CD8^{+} T cells from WT hosts or CD44^{hi} CD8^{+} T cells from *Fcgr2b*$^{-/-}$ hosts that were preincubated with media alone or anti-FcγRIIB (clone 2.4G2) and then stained with Fgl2. Summary data ±SEM are shown, n=4 replicates per group. Two-way ANOVA with multiple comparisons, ****p<0.0001.

(H-I) WT or *Fcgr2b*$^{-/-}$ OT-I CD8^{+} T cells isolated from the spleen were stimulated for 2 days with SIINFEKL peptide and then supplemented with 0.1 or 1.0ug/mL soluble Fgl2 for 24 hours.

H: The frequency of caspase 3/7^{+}7-AAD^{+} OT-I CD8^{+} T cells following stimulation with or without soluble Fgl2. Summary data ±SEM is shown. Pooled data from 3 independent experiments, n=2–3 per group. Two-way ANOVA with multiple comparisons, *p<0.05, **p<0.01.

I: The fold increase in cell number of caspase 3/7^{+} 7-AAD^{+} OT-I T cells following stimulation with or without soluble Fgl2. Summary data ±SEM is shown. Pooled data from 3 independent experiments, n=2–3 per group. Mann-Whitney test, *p<0.05.

See also Figure S2.

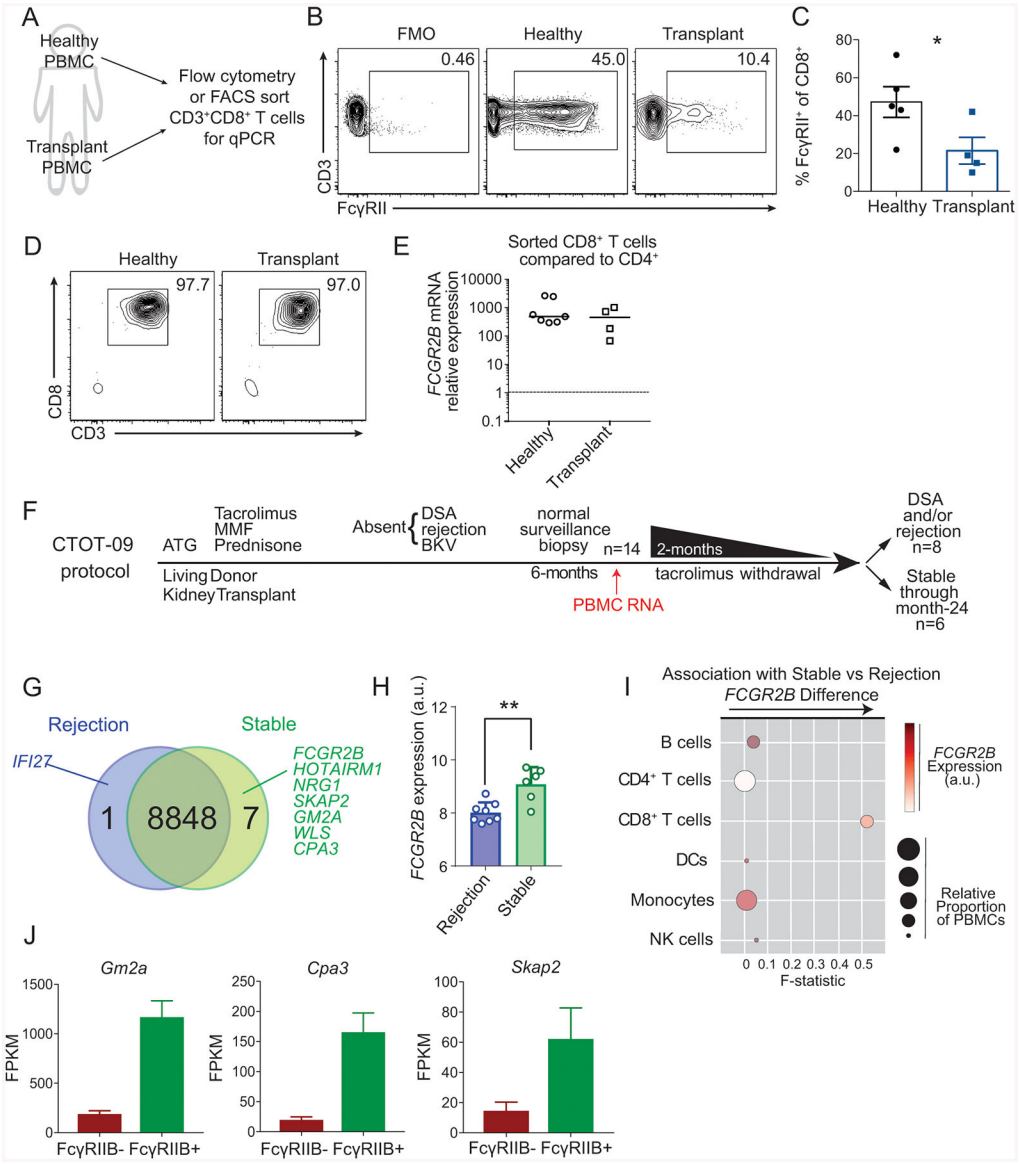

Figure 6: FcγRIIB is expressed on human CD8$^+$ T cells and is associated with freedom from rejection following withdrawal from tacrolimus immunosuppression in renal transplant recipients.

(A-E) A: Schematic of experimental design for B-E: PBMCs from healthy human subjects and renal transplant recipients were isolated for flow cytometry and sorting to perform qPCR of *FCGR2B*.

B: Representative flow cytometric plots of the expression of FcγRII on CD8$^+$ T cells in PBMCs from healthy human subjects and in renal transplant recipients.

C: The frequency of FcγRII$^+$ cells among CD8$^+$ T cells as shown in B. Summary data ±SEM are shown. n=5 healthy controls and n=4 transplant recipients. Mann-Whitney test, *p<0.05.

D: Flow cytometric plots of the purity of cells following FACS sorting of CD19$^-$CD14$^-$CD3$^+$CD4$^-$CD8$^+$ T cells from healthy and transplant recipients.

E: Relative expression ($2^{-\Delta\Delta CT}$) of *FCGR2B* normalized to internal *GAPDH* and to $CD4^+$ T cells from sorted $CD19^-CD14^-CD3^+CD4^-CD8^+$ T cells from healthy and transplant recipients.

(F-I) F: Schematic overview of the CTOT09 study analyzed in panels G-I. PBMC RNA was harvested prior to tacrolimus withdrawal and analyzed for differential gene expression.

G. Summary of differentially expressed genes from microarrays analyzing mRNA extracted from PBMCs of stable patients vs. patients that rejected. Upregulation logFc > 1.5, $p<0.001$.

H. *FCGR2B* expression in patients that rejected vs. those that were stable, $p<0.01$.

I. CellCODE analysis of microarray samples obtained before tacrolimus withdrawal. Data points depict the surrogate proportion variables (size) association, the average relative expression of *FCGR2B* across all the samples (color intensity), and its association with the difference in expression observed for each major subset between stable patients and patients that reject (x-axis, see *Methods*).

J: Fragments per kilobase per million (FPKM) of *Gm2a, Cpa3, and Skap2* in the $Fc\gamma RIIB^+$ and $Fc\gamma RIIB^-$ sorted OT-I T cells from the experimental design in Fig. 3F.

KEY RESOURCES TABLE

REAGENT or RESOURCE	SOURCE	IDENTIFIER
Antibodies		
BV785 anti-mouse CD8a antibody	BioLegend	BioLegend Cat# 100750, RRID:AB_2562610
PacBlue anti-mouse CD4 antibody	BioLegend	BioLegend Cat# 100428, RRID:AB_493647
PerCP anti-mouse Thy1.1 antibody	BioLegend	BioLegend Cat# 202512, RRID:AB_1595487
BV605 anti-mouse CD45.1 antibody	BioLegend	BioLegend Cat# 110738, RRID:AB_2562565
PE-Dazzle anti-mouse CD45.2 antibody	BioLegend	BioLegend Cat# 109846, RRID:AB_2564177
Biotin anti-mouse CD16/32 antibody, clone 2.4G2	BD Biosciences	BD Biosciences Cat# 553143, RRID:AB_394658
PE anti-mouse TCR Vb5 antibody	BioLegend	BioLegend Cat# 139504, RRID:AB_10613279
APC Streptavidin	BioLegend	BioLegend Cat# 405207
Biotin anti-mouse IgG2b k isotype control antibody	BD Biosciences	Cat# 553987, RRID:AB_10053772
FITC anti-mouse TCR Va2 antibody	BioLegend	BioLegend Cat# 127806, RRID:AB_1134188
BV605 anti-mouse CD3e antibody	BD Biosciences	BD Biosciences Cat# 564378, RRID:AB_2738779
BV510 anti-mouse CD19 antibody	BioLegend	BioLegend Cat# 115546, RRID:AB_2562137
BV510 anti-mouse CD14 antibody	BioLegend	BioLegend Cat# 123323, RRID:AB_2564129
FITC anti-mouse CD11c antibody	BioLegend	BioLegend Cat# 117306, RRID:AB_313775
APC-Cy7 anti-mouse CD44 antibody	BioLegend	BioLegend Cat# 103028, RRID:AB_830785
PE-Cy7 anti-mouse CD62L antibody	BioLegend	BioLegend Cat# 104418, RRID:AB_313103
FITC anti-mouse CD40 antibody	BioLegend	Biolegend Cat# 124610, RRID:AB_1134075
APC anti-mouse FcγRIIB (clone AT130)	eBiosciences	Ref# 17-0321-82
PE anti-mouse CD244 antibody	BD Biosciences	BD Biosciences Cat# 553306, RRID:AB_394770
BV711 anti-mouse CD69 antibody	BioLegend	BioLegend Cat# 104537, RRID:AB_2566120
PE anti-mouse Eomes antibody	BD Pharmingen	Cat# 566749
BV421 anti-mouse Tbet antibody	BioLegend	BioLegend Cat# 644815, RRID:AB_10896427
PE-Cy7 anti-mouse TNF antibody	BioLegend	BioLegend Cat# 506323, RRID:AB_2204356
AlexaFlour700 anti-mouse IFNγ antibody	BioLegend	BioLegend Cat# 505824, RRID:AB_2561300
BV421 anti-mouse IL-2 antibody	BioLegend	BioLegend Cat# 503825, RRID:AB_10895901
Fgl2 monoclonal antibody (clone 6D9)	Abnova	Abnova Cat# H00010875-M01, RRID:AB_565732
PE mouse IgG2a,k	BioLegend	BioLegend Cat# 400212
Caspase 3/7 kit	Thermofisher	Cat # C10427
V500 anti-human CD14	BD Pharmingen	BD Biosciences Cat# 562693, RRID:AB_2737727
V500 anti-human CD19	BD Pharmingen	BD Biosciences Cat# 561121, RRID:AB_10562391
BV510 anti-human CD14	BioLegend	BioLegend Cat# 301842, RRID:AB_2561946
BV510 anti-human CD19	BioLegend	BioLegend Cat# 302242, RRID:AB_2561668
BV711 anti-human CD8	BioLegend	BioLegend Cat# 344734, RRID:AB_2565243
V450 anti-human CD4	BD Pharmingen	BD Biosciences Cat# 560345, RRID:AB_1645572
PerCP-Cy5.5 anti-human CD3	BD Pharmingen	BD Biosciences Cat# 560835, RRID:AB_2033956
BV785 anti-human CD8	BD Pharmingen	BD Biosciences Cat# 563823, RRID:AB_2687487

REAGENT or RESOURCE	SOURCE	IDENTIFIER
APC-H7 anti-human CD4	BD Pharmingen	BD Biosciences Cat# 560158, RRID:AB_1645478
PE anti-human CD32 (FUN-2)	BioLegend	Cat# 303205, RRID:AB_314337
anti-mouse FcγRIIB (clone AT128)	Williams, et al., 2012. Dr. Mark Cragg	
InVivoMAb anti-mouse CD16/32 (clone 2.4G2)	BioXcell	Cat# BE0307, RRID:AB_2736987
Bacterial and Virus Strains		
Biological Samples		
Emory Transplant Center Biorepository	Emory IRB protocol #00046593	
Chemicals, Peptides, and Recombinant Proteins		
GolgiPlug	BD Biosciences	Cat# 555029
OVA peptide 257–264 (SIINFEKL)	GenScript	Cat# RP10611
CTLA-4Ig (abatacept)	Bristol-Myers Squibb,	Abatacept (Orencia)
Anti-CD28 domain antibodies	Bristol-Myers Squibb	
Collagenase (type 1A)	Sigma-Aldrich	C2654
Hyaluronidase (type 1)	Sigma-Aldrich	H3506
Collagenase P	Sigma-Aldrich	Ref# 11213865001
Collagenase D	Sigma-Aldrich	Ref# 1088866001
Recombinant Fgl2	R&D Systems	R&D Cat# 5257-FL-050
Critical Commercial Assays		
MACS CD8a+ T cell isolation kit, mouse	Miltenyi Biotec	130-104-075
Quick-RNA MicroPrep Kit	Zyma Research	R1051
SMART-seq v4 cDNA synthesis kit	Takara	Cat# 634894
NexteraXT kit	Illumina	FC-131–1096
Mouse Fgl2 ELISA	Biolegend	Biolegend Cat# 437807
RNeasy Plus Micro Kit	Qiagen	Qiagen Cat# 74034
High Capacity cDNA reverse transcription kit	ThermoFisher	ThermoFisher Cat# 4368814
HT HG-U133 Plus PM BeadChip	Affymetrix	Thermo Fisher Cat# 901261
Lightning Link R-PE Antibody Labeling kit	Novus Biologicals	Cat # 703–0010
CountBright Beads	Life Technologies	Cat # C36950
Deposited Data		

REAGENT or RESOURCE	SOURCE	IDENTIFIER
RNAseq data	NCBI Gene Expression Omnibus (GEO)	GSE118439
Experimental Models: Cell Lines		
B16 Melanoma-OVA	Brown, et al., 2001, provided by Dr. Yang-Xin Fu	
Experimental Models: Organisms/Strains		
NCI C57Bl/6Ncr (NCI grantee program)	Charles River	Stock #556
NCI B6-LY5.1/Cr (NCI grantee program)	Charles River	Stock #564
OT-I	Hogquist et al., 1994	
OT-II	Barnden et al., 1998	
mOVA (C57Bl/6 background, H-2b)	Ehst et al., 2013 Dr. Marc Jenkins	
B6.129P2-Aicda$^{tm1(cre)Mnz}$/J (*Aicda*$^{-/-}$)	The Jackson Laboratory	Stock #007770
B6;129S-Fcgr2btm1Ttk/J (*Fcgr2b*$^{-/-}$)	The Jackson Laboratory	Stock #002848
EM:06078 Fcgr2b Fcgr2bB6null B6(Cg)-Fcgr2btm12Sjv/Cnbc (*Fcgr2b*$^{-/-}$)	European Mutant Mouse Archive; Dr. J.S. Verbeek	EM: 06078
Fcgr2b$^{-/-}$ OT-I (bred from EM:06078 and OT-I)	This paper	N/A
Oligonucleotides		
Fcgr2b	Thermo Fisher	Hs00269610_m1, cat. # 4448892
Gapdh	Thermo Fisher	Hs02786624_g1, cat. # 4331182
Recombinant DNA		
Software and Algorithms		
TopHat2	Kim et al., 2013	
UCSC mm9 Known Gene	Hsu et al., 2009	
GenomicRanges (v1.22.4)	R/Bioconductor	
edgeR	Robinson et al., 2010	
Cytobank (viSNE)	Amir el et al., 2013	
Bioconductor	Gentleman, et al., 2004	
CellCODE	Chikina, et al., 2015	
Prism v7	Graphpad Software	
FlowJo (v9.9.4, v9.9.6)	Tree Star	
Other		

REAGENT or RESOURCE	SOURCE	IDENTIFIER